UPPSALA
UNIVERSITET

UPTEC E 25008
Examensarbete 30 hp
June 2024

# Modeling and Control System Design for European Balancing of Offshore Wind Power and HVDC Connections

Hampus Englund

Civilingenjörsprogrammet i elektroteknik

Modeling and Control System Design for European balancing of Offshore Wind Power and HVDC Connections

Hampus Englund


## Abstract

This thesis investigates how offshore wind farms connected via high-voltage direct current (HVDC) links can support frequency balancing between two synchronous areas in Europe. A simulation model was developed in MATLAB/Simulink to evaluate four control strategies for managing power imbalances caused by wind forecast errors. The strategies include routing the imbalance to one area, sharing it between both, or managing it locally at the wind farm with a simplified battery model. The model incorporates HVDC constraints, reserve limitations, and optional filtering of the imbalance signal.

Simulations using real wind data show that sharing the imbalance between areas results in the most optimal balancing control strategy. Routing all imbalances to a single area often causes HVDC saturation, ramping limitations, or insufficient frequency reserve. While local battery control can smooth short-term imbalances, it is not scalable for longer durations. The results highlight the importance of frequency reserve availability and HVDC transmission headroom for maintaining system stability, especially as offshore wind integration expands through more complex and interconnected grid systems.



**Teknisk-naturvetenskapliga fakulteten**

**Uppsala universitet, Utgivningsort Uppsala**

Handledare: Alicia Söderlind Ämnesgranskare: Robert Eriksson

Examinator: Saman Majdi

# Populärvetenskaplig sammanfattning

Utbyggnaden av havsbaserad vindkraft spelar en viktig roll i Europas omställning till förnybar elproduktion. I framtiden planeras nya lösningar där en och samma vindkraftspark kan kopplas till flera länder eller synkronområden. Dessa kopplingar, kallade *multi-purpose interconnectors* (MPIs), gör det möjligt att både överföra el från vindparken och balansera elnäten mellan länder. Det skapar nya möjligheter för effektivare resursanvändning, men också nya utmaningar när det gäller att hantera variationer i vindkraftsproduktionen.

Vid snabba förändringar i produktionen, till exempel på grund av väderomslag eller prognosfel, uppstår ofta obalanser i elsystemet. Dessa påverkar frekvensen i nätet och måste hanteras snabbt för att undvika störningar. I det här examensarbetet har en modell utvecklats i simuleringsverktyg MATLAB/Simulink för att undersöka hur sådana obalanser kan styras genom en vindkraftspark som är ansluten till två olika länder via HVDC-förbindelser.

Fyra kontrollstrategier har jämförts: att skicka all obalans till land A, till land B, att dela den mellan båda, eller att balansera lokalt vid vindkraftsparken med en förenklad batterimodell. Simuleringarna bygger på verkliga vinddata och tar hänsyn till både begränsningar i överföringskapacitet och hur snabbt kraftöverföringen får ändras (så kallade rampbegränsningar).

Resultaten visar att den bästa lösningen för att hantera obalanser är att dela den mellan båda länderna. Om all obalans skickas till ett enda land uppstår ofta problem, som att HVDC-förbindelsen blir överbelastad eller att frekvensreserverna inte räcker till. Den lokala batterilösningen fungerar för kortsiktiga variationer, men räcker inte till för längre obalanser.

Sammanfattningsvis visar arbetet hur olika styrstrategier påverkar stabiliteten i system med framtida havsbaserad vindkraft och HVDC-förbindelser. Det kan fungera som ett steg på vägen mot bättre förståelse för hur liknande lösningar i projekt för havsbaserad vindkraft kan planeras och utvärderas.

# Table of Contents

# Abbreviations

| | |
|---|---|
| aFRR | automatic Frequency Restoration Reserves |
| ENTSO-E | European Network of Transmission System Operators - Electricity |
| FCR | Frequency Containment Reserves |
| FFR | Fast Frequency Reserve |
| FRR | Frequency Restoration Reserves |
| HVDC | High Voltage Direct Current |
| ISA | Inter-Synchronous Area |
| LFC | Load Frequency Control |
| mFRR | manual Frequency Restoration Reserves |
| MPI | Multi-purpose Interconnector |
| TSO | Transmission System Operator |

# 1 Introduction

## 1.1 Background

Europe is currently undergoing a major transformation in its energy sector, driven by increasing electricity demand, energy security concerns, and climate goals. This transformation is accelerated by the electrification of transportation and industry, as well as the broader adoption of renewable energy technologies. Offshore wind power has emerged as a cornerstone in this transition, offering large-scale, land-efficient electricity generation.

The Northern Seas region is especially well-suited for offshore wind development due to its consistent wind resources and geographic proximity to population centers. According to ENTSO-E's TYNDP 2024 Sea-Basin Offshore Network Development Plan (ONDP), offshore wind capacity in Europe stood at 27 GW in 2025, with targets set at 119 GW by 2030 and 332 GW by 2050 [1]. This expansion aligns with the European Union's Green Deal and Clean Energy Package, both of which prioritize sustainable electricity generation and cross-border system integration.

To integrate this variable generation into the grid, High Voltage Direct Current (HVDC) systems are used for their efficiency in long-distance transmission and ability to connect asynchronous networks. Future offshore grid development involves Multi-Purpose Interconnectors (MPIs), which combine offshore wind integration with cross-border interconnection between synchronous areas. These systems, outlined in ENTSO-E and Svenska kraftnät planning documents [1] [2], improve resilience, enable efficient resource sharing, and support frequency stability. However, they also introduce increased complexity in system control.

Wind power variability—caused by forecast errors, rapid weather changes, storms, or wind ramp events—creates power imbalances that impact system frequency and challenge operational security, especially when offshore wind farms span multiple Load-Frequency Control (LFC) areas. Figure 1 provides an overview of the planned and potential offshore grid development in Europe, as described in ENTSO-E's Offshore Network Development Plan [3]. It highlights both existing and proposed hybrid and radial links, as well as key corridors identified for integrating offshore wind. This coordinated infrastructure expansion reflects a broader shift toward a more interconnected and resilient European electricity system, capable of balancing renewable variability across borders. Managing these fluctuations in a reliable, automated, and cost-effective manner remains crucial for maintaining system stability [4].

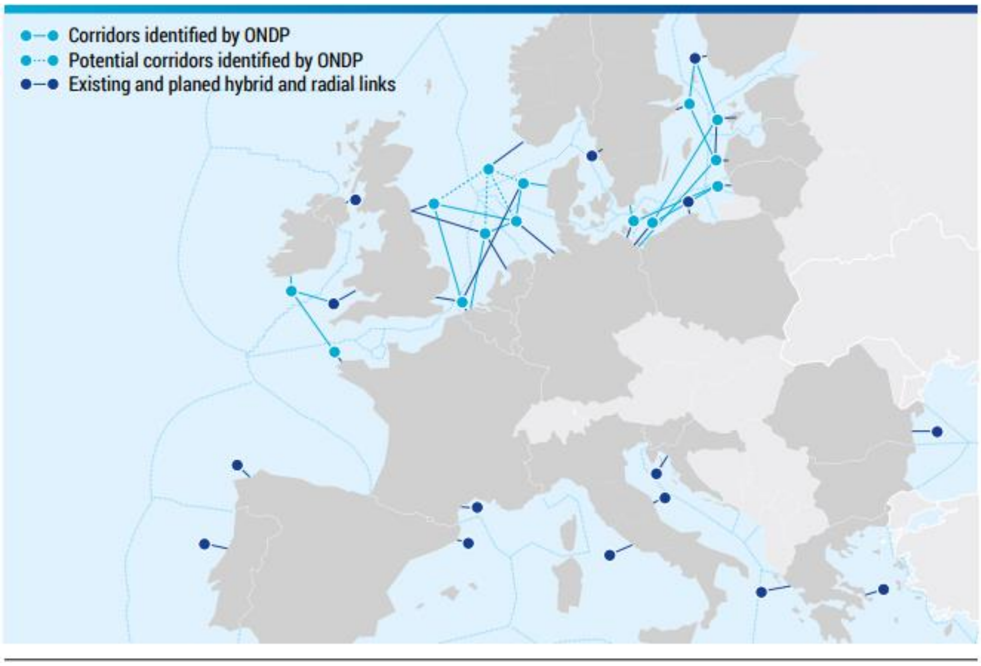


Figure 1. Existing, planned, and potential offshore hybrid and radial transmission links in Europe. Corridors and nodes are based on ENTSO-E's Offshore Network Development Plan [3].

## 1.2 Research Problem

The core research problem explored in this thesis is the development of a dynamic balancing model that reflects how offshore wind farms, connected via HVDC links, can support frequency stability between two synchronous areas. The work is grounded in the aim to develop generic building blocks within MATLAB/Simulink that represent critical components of the European transmission network—specifically HVDC links, offshore wind farms, and the LFC areas to which they are connected.

This thesis focuses on one integrated model: an offshore wind farm connected via two HVDC links to two LFC areas. This configuration allows for a focused, yet representative investigation of how future MPIs may operate in balancing contexts across European power systems.

The model is used to investigate the size of normal imbalances from offshore wind, how normal production variations in offshore wind power impact balancing capabilities and grid stability. Key focus areas include the LFC area's response to handle imbalances from offshore wind, the effects of distributing these imbalances through HVDC links, and the potential for local management at the wind farm using simulated control strategies. The objective is to determine how such systems can affect system balance and frequency stability under typical operating conditions.

## 1.3 Thesis objectives

The main objective of this thesis is to develop a simulation model in MATLAB/Simulink that represents a simplified section of the European transmission system. This model consists of an offshore wind farm connected via HVDC to two synchronous areas and is designed to reflect future configurations involving MPIs.

In support of this objective, the thesis aims to:

1. Analyze how normal production variations in offshore wind affect system balance and frequency stability.

2. Implement and evaluate control strategies for handling normal imbalances from offshore wind—either by distributing them between synchronous areas or by simulating local mitigation, considering cases both with and without local frequency control, as FCR, at the wind farm.

3. Estimate the energy storage or regulation capacity needed at the wind farm, to handle these imbalances effectively.

## 1.4 Scope

The study is limited to a representative model of one offshore wind farm connected via HVDC links to two LFC areas. While this simplifies the broader European vision involving interconnected MPIs across multiple regions, it provides a foundational analysis of control, balancing, and capacity allocation challenges relevant to grid operators and transmission planners.

The selected scenarios cover a range of imbalance types derived from real wind production and forecast data, ensuring that results are grounded in operationally relevant conditions.

In all simulations, the system is configured for a desired power import of 2 GW into one of the synchronous areas (LFC Area A). This fixed import assumption provides a consistent baseline for evaluating system response under varying control and imbalance scenarios.

The research will focus on balancing models involving two LFC areas interconnected by HVDC links, rather than multiple interconnected areas, as a starting point for understanding the complexities involved in balancing energy production in such systems.

## 1.5 Disposition

- **Chapter 1: Introduction** – Presents the background, research question, and scope.

- **Chapter 2: Background** – Describes the core technical concepts including HVDC systems, MPIs, grid balancing mechanisms, and wind power dynamics. including HVDC systems, MPIs and grid balancing mechanisms.

- **Chapter 3: Methodology** – Details model development, simulation parameters, data processing, and control setup.

- **Chapter 4: Results and Analysis** – Summarizes outcomes for various imbalance and control configurations.

- **Chapter 5: Conclusion and Recommendations** – Concludes with key insights, implications, and suggestions for future work.

# 2 Background

## 2.1 Load-Frequency Control (LFC) Areas and Blocks

Stable frequency control (50 Hz in Europe) is essential for secure grid operation. The European system achieves this through a layered LFC structure. Each **LFC Area**, managed by a TSO, is responsible for balancing internal load and generation while maintaining scheduled power exchanges with neighbors.

The LFC framework consists of:

- **Frequency Containment Reserves (FCR)**: Immediate response to frequency deviations (activation time within 30 seconds) [4].
- **Automatic Frequency Restoration Reserves (aFRR)**: Activated to restore frequency and inter-area exchange schedules (activated within several minutes) [4].
- **Manual Frequency Restoration Reserves (mFRR)**: Manually dispatched reserves for sustained deviations [4].

The central performance metric is the **Area Control Error (ACE):**

$$ACE = \Delta P_{\mathrm{tie}} + B \cdot \Delta f$$

Where:

- $\Delta P_{\mathrm{tie}}$ is the deviation in tie-line power flows,
- $B$ is the frequency bias factor in MW/Hz,
- $\Delta f$ is the frequency deviation from 50 Hz [5].

LFC Blocks group multiple LFC Areas to coordinate the activation of Frequency Restoration Reserves (FRR) and Replacement Reserves (RR), improving cross-regional robustness. Control responses are typically implemented using Proportional-Integral (PI) controllers, designed based on the dynamic characteristics of reserve providers [6].

## 2.2 Multi-Purpose Interconnectors (MPIs)

MPIs combine offshore wind integration with cross-border HVDC interconnection. They serve dual roles: facilitating renewable integration and enabling dynamic energy exchange across synchronous areas.

According to ENTSO-E and Svenska kraftnät [1] [2]:

- MPIs enable optimized reserve sharing and congestion relief.
- They reduce renewable curtailment and improve asset utilization.
- They support enhanced frequency stability by distributing imbalances across regions.

The complexity of MPI operation stems from the need for coordinated control, transmission rights allocation, and compatibility between regional balancing markets. Advanced coordination mechanisms and real-time control strategies are essential to fully exploit MPI functionality.

## 2.3 Imbalance Dynamics and Reserves

Imbalances occur when generation does not match load, leading to frequency deviations. In wind-dominated systems, these are largely caused by wind speed variability, forecasting errors, and rapid weather shifts.

Relevant reserves for imbalance management include:

- **FCR**: Immediate correction to arrest frequency deviation [4].
- **aFRR**: Automated control to restore normal operation [4].
- **mFRR**: Activated by system operators for significant, prolonged imbalances [4].
- **FFR** (Fast Frequency Reserve): A newer category aimed at handling steep frequency drops in low-inertia systems [2].

The model uses first-order filtering techniques to separate the fast and slow components of the imbalance signal. High-frequency components can be absorbed locally (e.g., by wind turbine control systems or batteries), while low-frequency trends are redistributed via HVDC links for coordinated correction [2] [4].

## 2.4 Wind Power Fundamentals

Wind turbines convert kinetic energy into electrical power based on:

$$P = \frac{1}{2} \cdot \rho \cdot A \cdot v^3$$

Where:

- $\rho$ is the air density,
- $A$ is the swept area of the rotor,
- $v$ is the wind speed.

The cubic dependence on wind speed means that small changes in wind conditions can lead to large variations in power output. This variability poses a major challenge for system balancing and necessitates robust control mechanisms. Furthermore, forecast errors—even when small in magnitude—can propagate through the nonlinear power–wind speed relationship, resulting in disproportionately large deviations from expected generation and complicating operational planning and reserve allocation.

Wind farms must implement curtailment strategies, pitch control, and fast-reacting control systems to contribute to frequency stability. When integrated via MPIs and HVDC, they become active participants in balancing, not just passive generators [7].

# 3 Methodology

## 3.1 MATLAB/Simulink Modeling Framework

The core of this thesis is a simulation model developed using **MATLAB R2024a** and **Simulink**, designed to represent and analyze interactions within a hybrid energy system, which includes a wind farm, imbalance filtering, a control strategy, HVDC links, and two LFC areas. The model's main components were structured as modular subsystems to support testing and potential future extension. Control blocks, filters, and HVDC constraints were implemented using standard Simulink libraries, while custom MATLAB scripts handled data management, scenario configuration, automated simulation execution, and output processing. This integrated modeling approach offers a flexible and transparent framework appropriate for investigating dynamic behaviors in power systems.

### 3.1.1 Wind Farm Model

The wind farm serves as the central energy producer in the system, situated between two LFC areas—referred to as LFC A and LFC B. These areas alternate roles as energy importers or exporters depending on the simulation scenario. Wind power generation is based on real-world forecast and production data sourced from an actual wind park, scaled to 2 GW to represent the characteristics of offshore wind power. Due to data confidentiality, specific sources cannot be disclosed.

The difference between the forecasted and actual power output represents the wind farm's imbalance. This imbalance is a key input to the filtering and control mechanisms described below.

### 3.1.2 Imbalance Filtering

The model includes an optional filtering stage that separates fast and slow components of the wind farm power imbalance signal caused by wind forecast errors. This conceptual filter represents the idea that different parts of the imbalance could be handled by different control resources, depending on their frequency content—with faster variations potentially managed by FCR, and slower variations by FRR.

In principle, rapid fluctuations are better suited for local balancing mechanisms — such as wind turbine control or on-site storage—while slower variations can be routed to central controllers through HVDC links. By separating the signal into high- and low-frequency components, the model enables simulation of this division of control responsibility.

### 3.1.3 Imbalance Control Strategy

The control system offers four configuration modes to manage imbalances:

1. Route all imbalances to LFC area B.
2. Route all imbalances to LFC area A.
3. Distribute imbalances between LFC area A and B using a predefined key distribution factor.
4. Retain all imbalances locally (representing idealized battery control).

For mode 3, a sharing key of 70% to LFC B and 30% to LFC A was selected. This split was chosen primarily to create an interesting case study and does not have a basis in real-world operational data or agreements.

In mode 4, although batteries are not modeled as physical batteries, the required storage capacity is estimated by integrating the imbalance over time, yielding an approximation of the necessary energy storage capacity to fully manage imbalances locally.

### 3.1.4 HVDC Link Model

The HVDC links connecting the wind farm to the LFC areas are modeled with two primary constraints:

- **Saturation Limit**: Simulates the maximum transmission capacity of the link.
- **Ramp Rate Limiter**: Models limitations in how quickly power can be increased or decreased over time.

The model tracks both the total energy input and output of the HVDC links. If energy cannot be transmitted due to these constraints, the model flags the occurrence as an overload under the current simulation parameters. Note that the model does not account for HVDC transmission losses or possible overcapacity.

### 3.1.5 Load Frequency Control (LFC) Areas

The LFC area models were adapted from templates provided by international research collaborators and modified to suit the purposes of this study. Each LFC area receives imbalances routed from the wind farm, generating a local ACE. A built-in PI controller responds to the ACE by requesting FRR, specifically aFRR, from available providers.

The list of providers and their characteristics is based on a survey conducted among real TSOs. These providers are then activated in the model in response to the aFRR requests generated by the LFC controller.

### 3.1.6 Simulation Parameters

Each simulation covers 15 minutes, with one data point per second. The 15-minute duration is chosen to accurately simulate the activation and response of aFRR. The one-second resolution ensures sufficient accuracy in capturing fast-changing imbalance dynamics.

## 3.2 Data Collection

The dataset used in this study was provided by the ISA working group within the ENTSO-E organization. To reflect the scale and dynamics of the system under consideration, the data were scaled accordingly to represent realistic production volumes and their associated imbalances.

Two types of data were made available: forecasted production values and actual (realized) production data. The forecasted data were updated on the same day, with each forecast issued one hour prior to the corresponding real-time interval. Forecasted values were provided at hourly intervals, while the realized production data were sampled every 10 seconds. To enable consistent and high-resolution analysis, both datasets were interpolated to achieve a common time series with a resolution of one data point per second.

This process was applied to three distinct one-hour periods, each originating from a different wind farm. Each hour was divided into four 15-minute segments, from which a total of five quarters were selected for simulation. These segments were chosen to represent a range of imbalance scenarios relevant to system performance under varying operational conditions:

1. **Quarter 1:** Characterized by minimal imbalance, the actual production fluctuates slightly between overproduction and underproduction, eventually trending increasingly negative by the end of the interval.

2. **Quarter 2:** Displays a significant overproduction lasting for nearly four minutes, followed by a shift into sustained underproduction for the remainder of the segment.

3. **Quarter 3:** Begins with a small underproduction that gradually intensifies, ending with a substantial negative imbalance.

4. **Quarter 4:** Features actual generation that starts at approximately 1000 MW and decreases to around 950 MW, with fluctuations reaching as high as 1050 MW and as low as 900 MW. In contrast, the forecasted production increases from 900 MW to about 1050 MW, resulting in an initial overproduction that transitions into underproduction.

5. **Quarter 5:** Involves a relatively steady actual generation at around 900 MW, while the forecasted production starts at 1200 MW and increases to 1300 MW. This leads to a steadily growing negative imbalance throughout the quarter.

These five scenarios were selected to capture a diverse set of imbalance profiles, including transitions between over- and underproduction, gradually intensifying imbalances, and relatively stable production mismatched with dynamic forecasts. Together, they form a basis for evaluating the system’s response and the effectiveness of mitigation strategies under different realistic operating conditions. The plots are shown in 4.1.

## 3.3 Assumptions and Limitations

While the model is designed with considerable flexibility—allowing for adjustments in system parameters, control strategies, and interconnection configurations, this study focuses on a specific scenario to ensure clarity and relevance. In all simulations, the market flow was set to a fixed import of 2 GW into LFC Area A. This assumption provides a consistent baseline and reflects one of the possible operating conditions anticipated in future offshore grid configurations.

The LFC area data used in the model was provided by the ENTSO-E ISA working group and is based on a survey conducted in 2018. While several parameters have been updated since then, the core structure remains consistent with the original dataset. This ensures transparency and traceability but also introduces a limitation: real-world configurations and reserve dynamics may have evolved, and using more recent data might influence certain outcomes.

The wind farm was modeled as an aggregated power source using scaled real-world forecast and production data. Detailed wind turbine dynamics, such as pitch control, inertia emulation, or local frequency support, were not included. As a result, the model does not capture fast-reacting control behavior at the wind turbine level.

The HVDC links connecting the wind farm to the LFC areas include ramp rate limitations to reflect realistic operational constraints. A ramping limit of 100 MW per minute was applied, based on specifications outlined in Elia Transmission Belgium's operational agreement for interconnectors between the Belgian and British synchronous areas [8]. This value was chosen to accurately represent the expected operational characteristics of offshore HVDC links in the Northern Seas region.

The LFC model used in this study focuses on aFRR as the primary balancing mechanism. mFRR are not included, and no additional disturbances—such as load variations or external events—are considered. Each LFC area is assumed to maintain a constant nominal frequency of 50 Hz throughout the simulations. This simplification enables a focused analysis of the wind power imbalance and its interaction with automated control responses, while acknowledging that real-world systems involve additional dynamics not captured in this model.

Additionally, the model architecture supports alternative scenarios—including variable market flows, different wind farm sizes, and expanded multi-area configurations—such explorations fall outside the scope of this thesis. Future research could build on this work by exploring more diverse configurations using the same modular framework.

## 3.4 Validation

The model was validated through a combination of structural verification and qualitative behavioral analysis. As the LFC blocks were externally provided and are assumed to be correctly implemented based on their prior use in validated models.

The remaining parts of the model—including wind generation dynamics, imbalance filtering, control logic and HVDC transmission constraints—were developed as part of this thesis and tested stepwise. Each subsystem was validated individually using simple test signals and constant inputs with known behavior, to confirm that outputs responded as expected. This step-by-step approach helped identify errors early and ensured the model behaved as intended.

## 3.5 System Overview

Figure 2 provides a conceptual overview of the simulated system architecture. The offshore wind farm is connected via two HVDC links to two separate synchronous areas, represented by LFC A and LFC B. Each LFC area includes local frequency control and reserve activation logic for aFRR. The HVDC links enable active balancing by transferring filtered or unfiltered power imbalances from the wind farm to one or both LFC areas, depending on the selected control strategy.

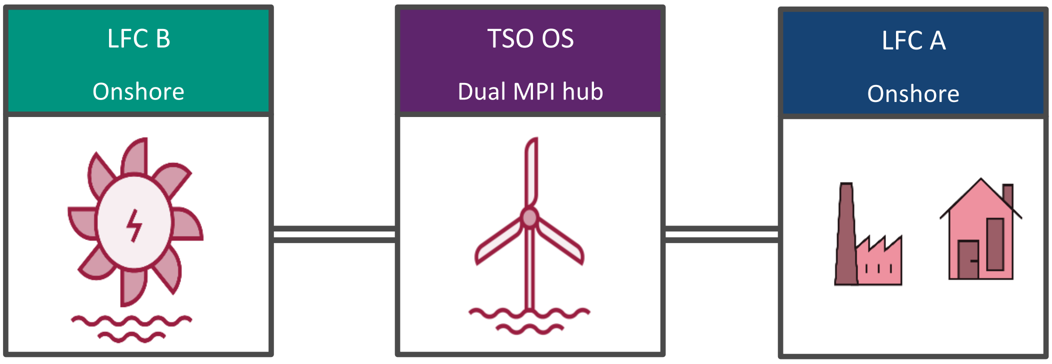


Figure 2. Conceptual overview of the simulated system architecture.

# 4 Results and Analysis

## 4.1 Input Data

To provide a clear foundation for the simulation study, the following figures present the selected input datasets used to drive the model. Each figure corresponds to a specific 15-minute interval of wind power production and displays the forecasted values, the actual (realized) output, and the resulting power imbalance. The dataset labels follow the format "DATA X.Y," where *X* denotes the hour and *Y* the quarter within that hour (e.g., DATA 1.3 refers to the third quarter of hour one). The selected intervals cover a diverse set of operational conditions, including persistent underproduction, short-term overproduction events, and gradually shifting imbalances. This variety ensures that the control strategies are evaluated under realistic and representative scenarios. The visual comparisons between forecasted and actual power highlight the dynamic nature of the system and contextualize the imbalance signals that the proposed control methods are designed to address.

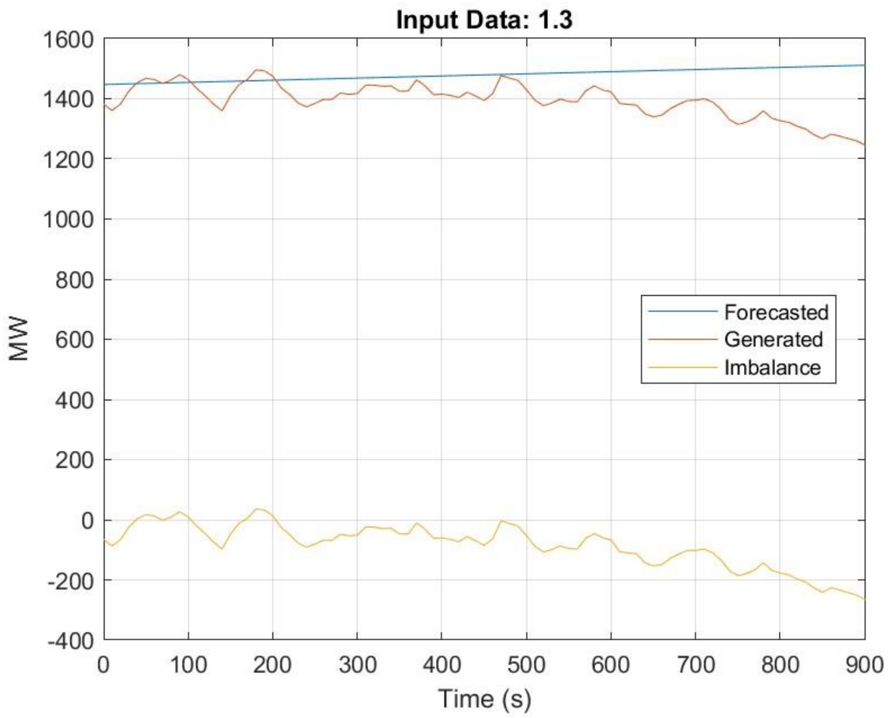


Figure 3. First dataset. Data 1.3.

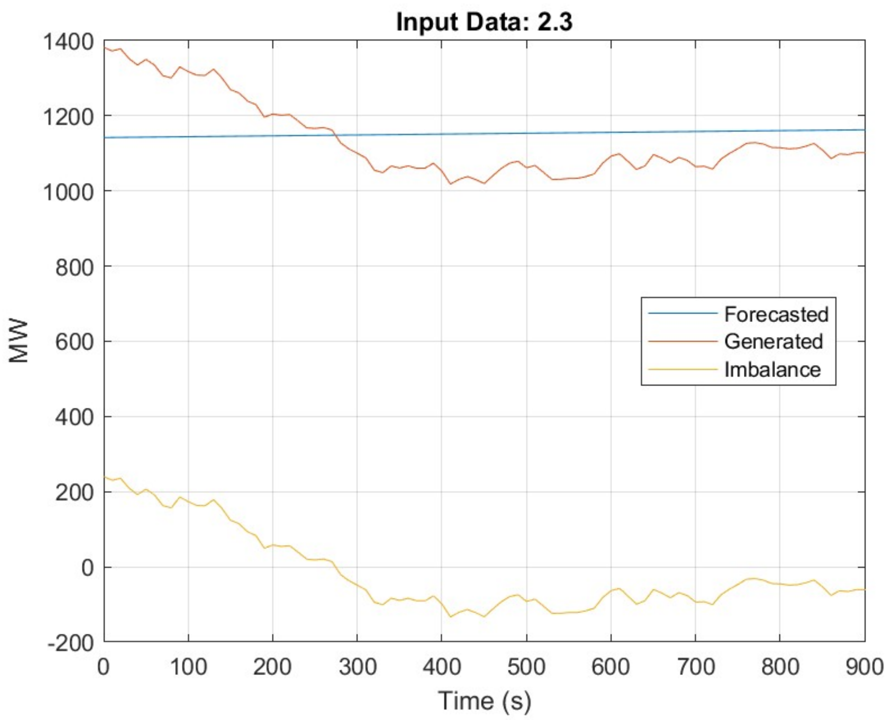


Figure 4. Second dataset. Data 2.3.

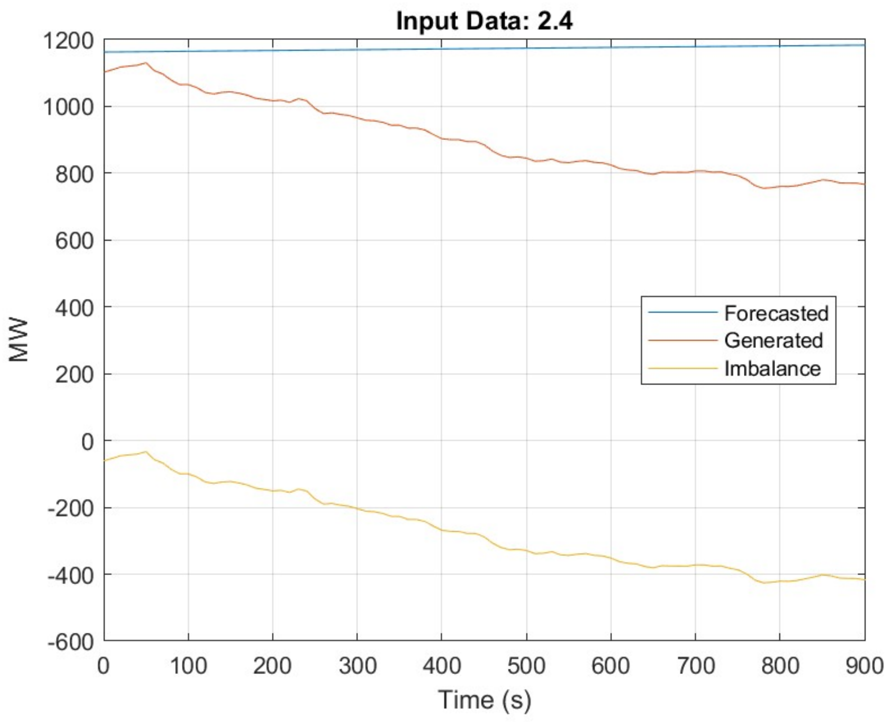


Figure 5. Third dataset. Data 2.4.

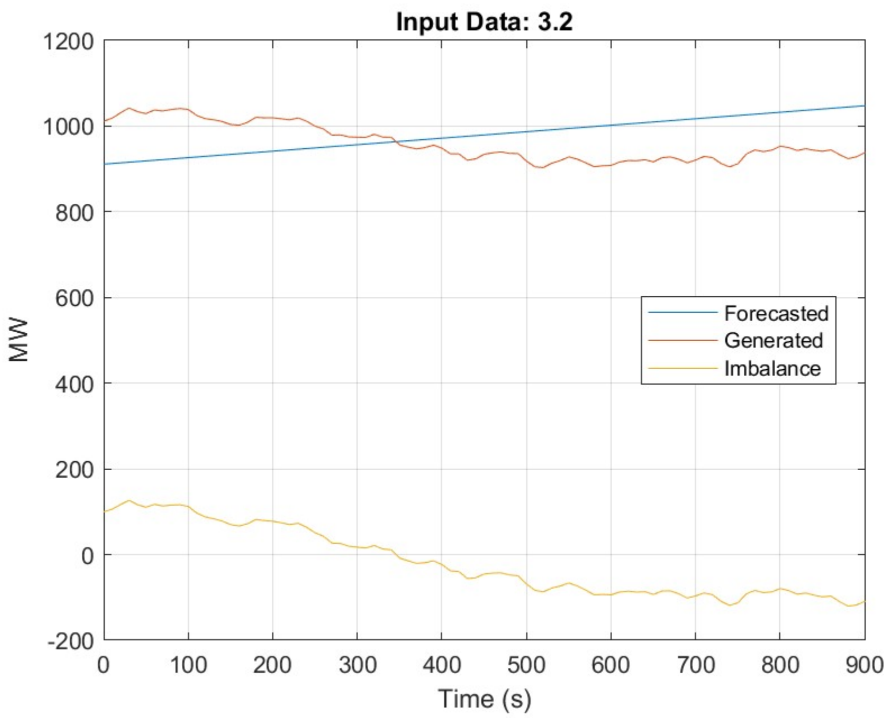


Figure 6. Fourth dataset. Data 3.2.

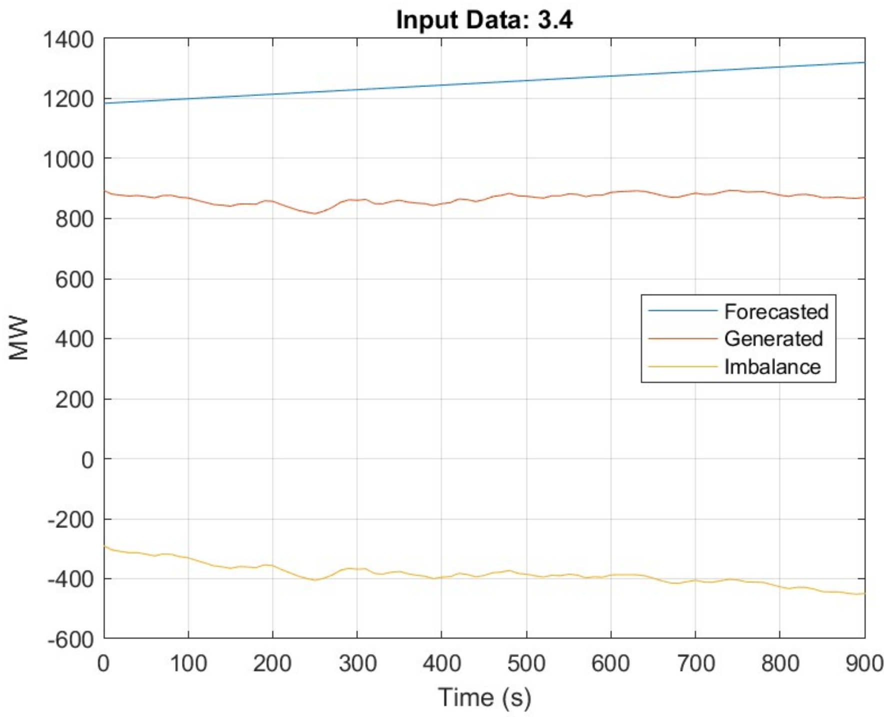


Figure 7. Fifth dataset. Data 3.4.

## 4.2 Filter selection

The effect of different filter durations on system behavior is shown in the following plots. Three filter settings are examined: 2 minutes, 5 minutes, and 10 minutes. As the filter duration increases, a clear smoothing effect is observed in both the ACE signal within the LFC area and the imbalance dynamics at the wind farm. The top plots illustrate how the ACE signal becomes progressively less volatile with longer filter durations, indicating a reduction in high-frequency control activity by the LFC. The bottom plots show that the total imbalance handled by the wind farm also becomes smoother as filter duration increases, although low-frequency deviations remain prominent. This behavior reflects the filter's role in partitioning the imbalance: the high-frequency components are passed to the LFC controller, while the low-frequency components are retained and handled at the wind farm. With longer filters, a larger share of the imbalance remains local, effectively shifting more control responsibility to the wind farm.

A filter duration of 5 minutes was selected for the remaining simulations, as it most realistically aligns with the response timescales of aFRR and the sustained effect window of FCR, both typically activated within 30 seconds to 5 minutes following a frequency deviation [4]. Although 2- and 10-minute filters are less representative of standard operational settings, they were included to explore the effects of different filters. This variation also provides a foundation for identifying trade-offs and potential avenues for future research, particularly regarding advanced local control strategies or battery integration.

To illustrate the effects of different filter durations, the results for 2-minute and 5-minute filters are presented below, as they represent the most relevant operational timescales. Results for the 10-minute filter, included for comparison, are provided in the Appendix.

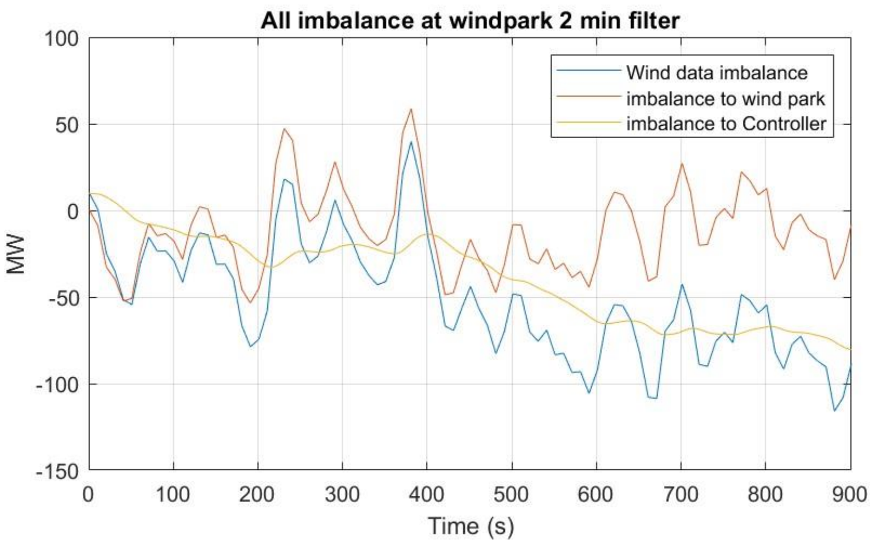


Figure 8. Two-minute filter length imbalance split.

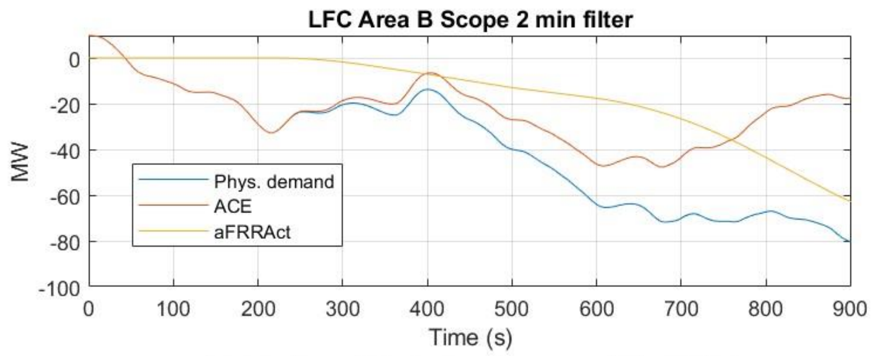


Figure 9. Two-minute imbalance at the LFC area.

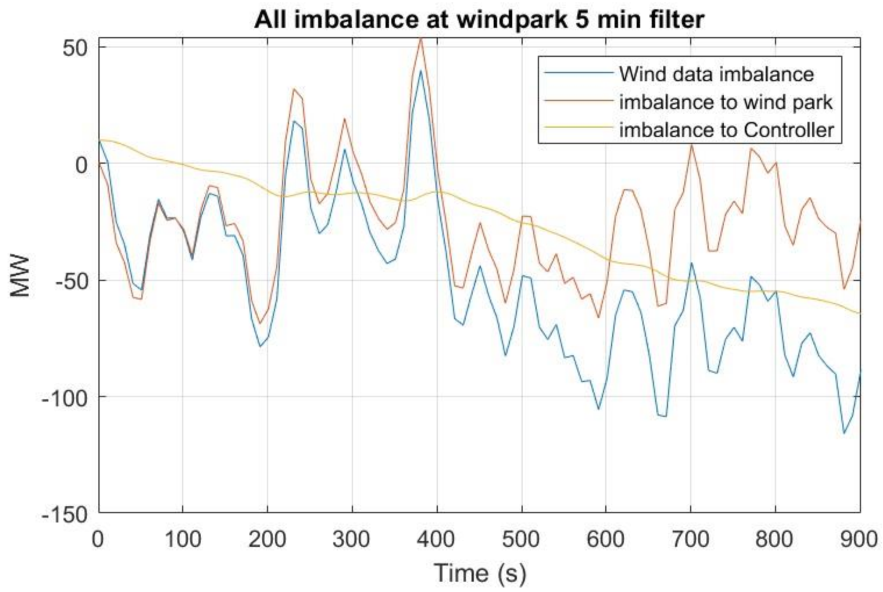


Figure 10. Five-minute imbalance split.

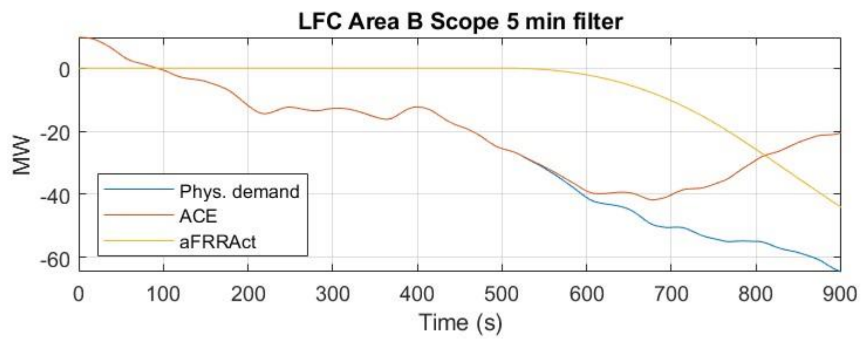


Figure 11. Five-minute imbalance at the LFC area.

## 4.3 Filtered Data

The following figures illustrate the results of applying a low-/high-pass filter to the wind power imbalance signal across five selected simulation cases. The filtering process uses a 5-minute time constant, in line with typical response times FRR. In each case, the original imbalance signal (shown in blue) is decomposed into two components: a low-frequency portion (brown) that remains at the wind farm, and a high-frequency portion (yellow) that is transferred to the central controller for balancing in the LFC areas via HVDC links.

This filtered representation provides insight into the dynamic allocation of control responsibility. In scenarios characterized by more gradual imbalance trends—such as those seen in Figure 24 and Figure 25—a larger portion of the imbalance is retained locally at the wind farm. Conversely, cases exhibiting faster fluctuations, such as seen in Figure 12, result in a greater share of high-frequency content being routed to the central controller. This division supports a practical control strategy in which fast, localized variations are managed near the point of generation, while slower, system-wide trends are coordinated centrally. Such an approach reduces the activation burden on central reserves and emphasizes the potential role of local flexibility assets, such as battery storage or responsive wind turbine controls.

To demonstrate how the filtering mechanism separates imbalance signals into high- and low-frequency components, the first dataset is shown below. The remaining cases, which exhibit similar trends under varying conditions, are available in the Appendix for reference.

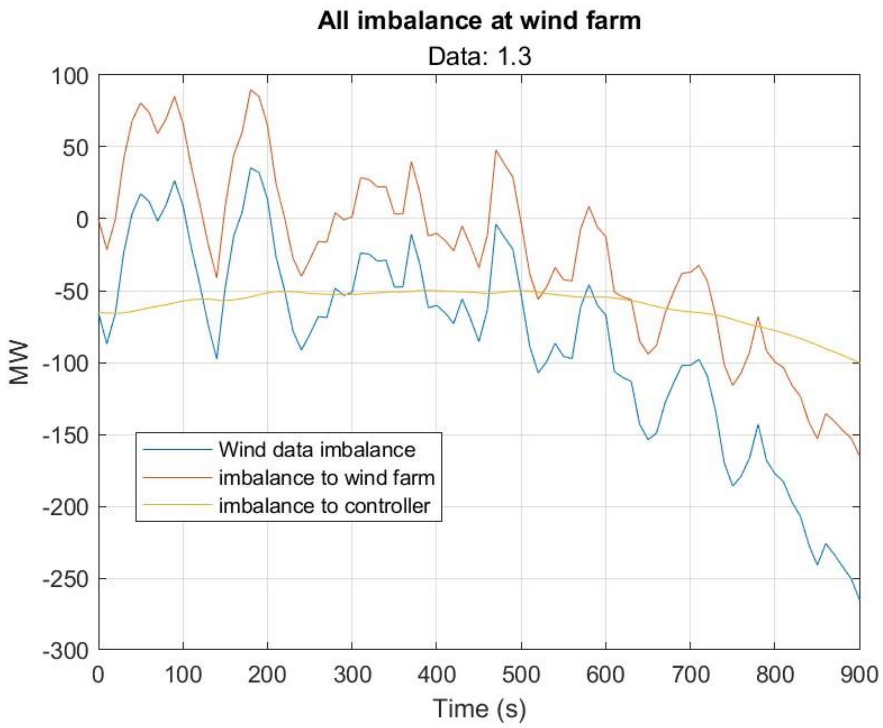


Figure 12. Filtered data 1.3.

## 4.4 Control alternatives

Before presenting the simulation results, this section outlines the four control strategies used to distribute the power imbalance caused by wind forecast errors. These strategies determine how the imbalance is allocated between the two connected LFC areas or handled locally:

1. **All to LFC area B** – The entire imbalance is handled by LFC Area B, while Area A receives only the scheduled market flow.
2. **All to LFC area A** – The entire imbalance is routed to LFC Area A, requiring this area to fully absorb both surplus and deficit power.
3. **Split (70/30)** – The imbalance is shared between the two areas, with 70% sent to LFC area B and 30% to LFC area A.
4. **Local Battery reserve** – The imbalance is handled locally by the offshore wind hub using a simplified battery model.

Each strategy is evaluated under identical wind scenarios to assess their impact on frequency control, HVDC load, and reserve activation in both areas.

To ensure readability while capturing the essential dynamics of each control strategy, only some representative datasets are shown per alternative. The full set of simulation results, including additional datasets for each strategy—can be found in the Appendix.

### 4.4.1 Alternative 1: All to LFC area B

In this configuration, all imbalances are directed solely to LFC area B.

**Key Findings Alternative 1**

In the configuration where all imbalances are routed to LFC area B, the system generally achieves stable operation. The ACE is effectively reduced in most scenarios. This is largely due to the relatively large aFRR capacity available in LFC B, which allows the area to absorb significant imbalance without saturating. Although HVDC link B experiences some minor overloads, these are typically below operational concern when considering real-world HVDC losses, which are not modeled here. Filtering improves the control signal smoothness and slightly enhances the system's ability to converge ACE, but is not essential for this alternative to succeed.

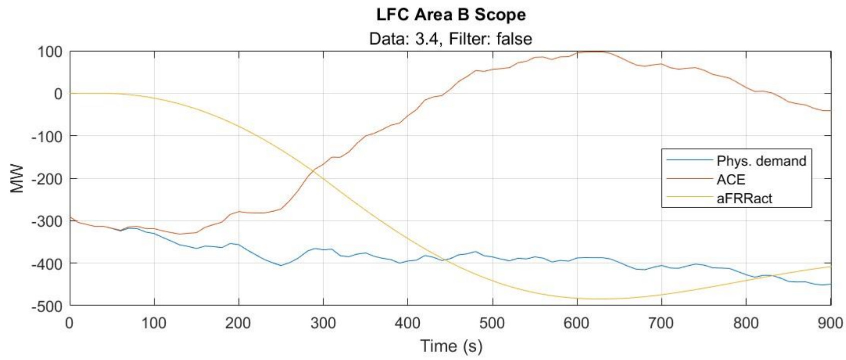


Figure 13. Alternative 1, data 3.4, no filtering, LFC area B.

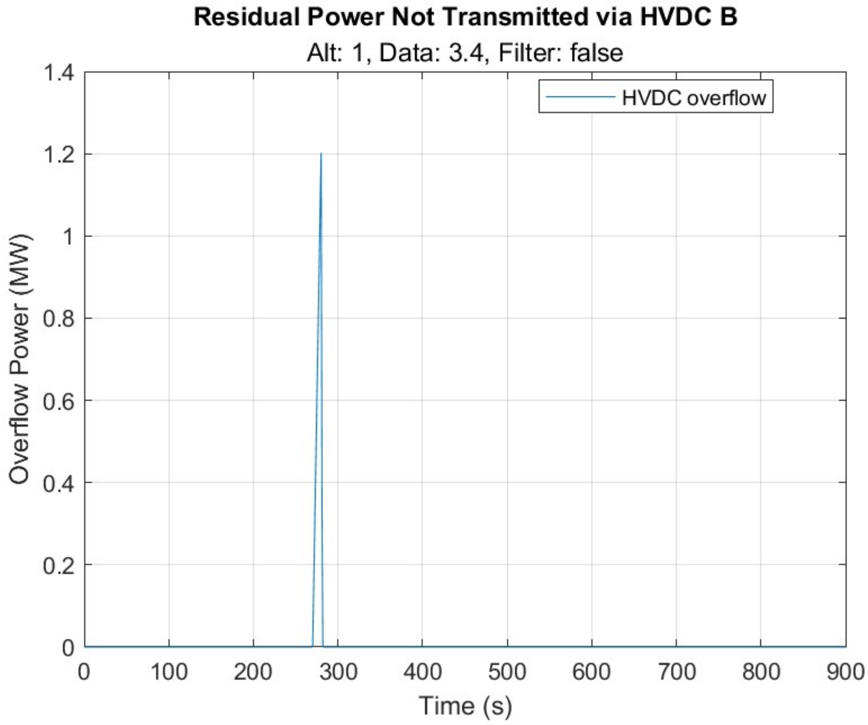


Figure 14. Alternative 1, data 3.4, no filtering, residual power.

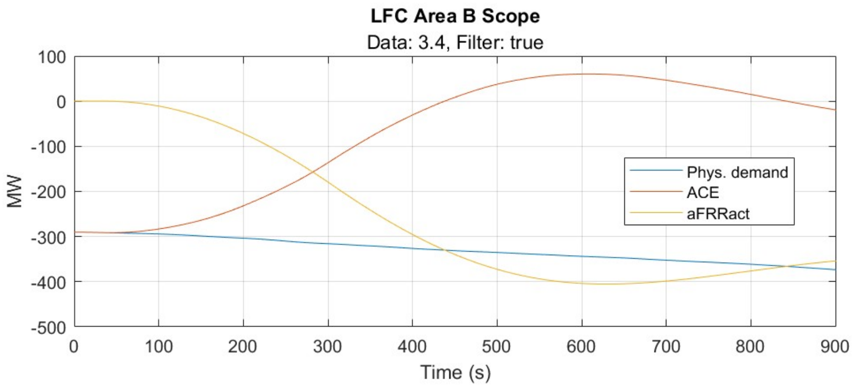


Figure 15. Alternative 1, data 3.4, filtering, LFC area B.

### 4.4.2 Alternative 2: All to LFC area A

This configuration assigns all imbalances to LFC area A.

**Key Findings Alternative 2**

Routing all imbalances to LFC area A introduces more pronounced limitations. The fixed 2 GW market flow saturates HVDC link A during overproduction conditions, meaning excess energy cannot be transferred. The limited aFRR capacity in LFC area A means that even when some imbalances are successfully routed, the area is often unable to fully correct the resulting ACE. Underproduction is managed more effectively due to available HVDC link headroom in that direction. Filtering smooths the response and provides some benefit, but cannot resolve the fundamental constraint of transmission capacity. One potential approach to alleviate this limitation is to reduce the scheduled market flow, thereby reserving headroom for imbalance correction. Alternatively, increasing the cable capacity of the HVDC link could directly address the bottleneck, allowing greater flexibility in energy transfer and improving overall system response.

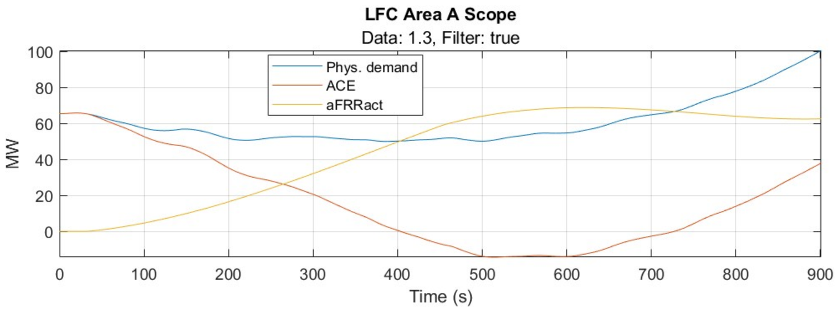


Figure 16. Alternative 2, data 1.3, filtering, LFC area A.

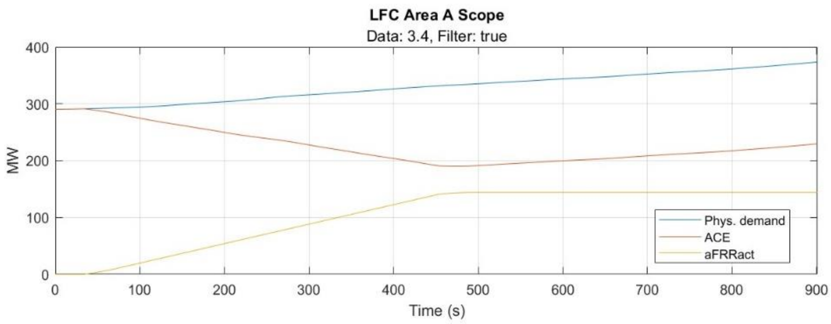


Figure 17. Alternative 2, data 3.4, filtering, LFC area A.

### 4.4.3 Alternative 3: Split between LFC area B & LFC area A

For this configuration, imbalances are shared between LFC area B and LFC area A, with a split of 70% to LFC area B and 30% to LFC area A.

**Key Findings Alternative 3**

Sharing the imbalance between LFC area B and LFC area A yields the most balanced performance across the tested scenarios. It avoids the extreme overload conditions seen in Alternatives 1 and 2 by distributing the burden. While HVDC link A is still vulnerable to saturation during overproduction due to the fixed 2 GW import, LFC area B's reserve capacity supports the overall response. The ACE is smoother and lower in magnitude, particularly when filtering is applied. Nonetheless, the effectiveness of this configuration still depends on the availability of headroom on the HVDC links and sufficient aFRR within both LFC areas.

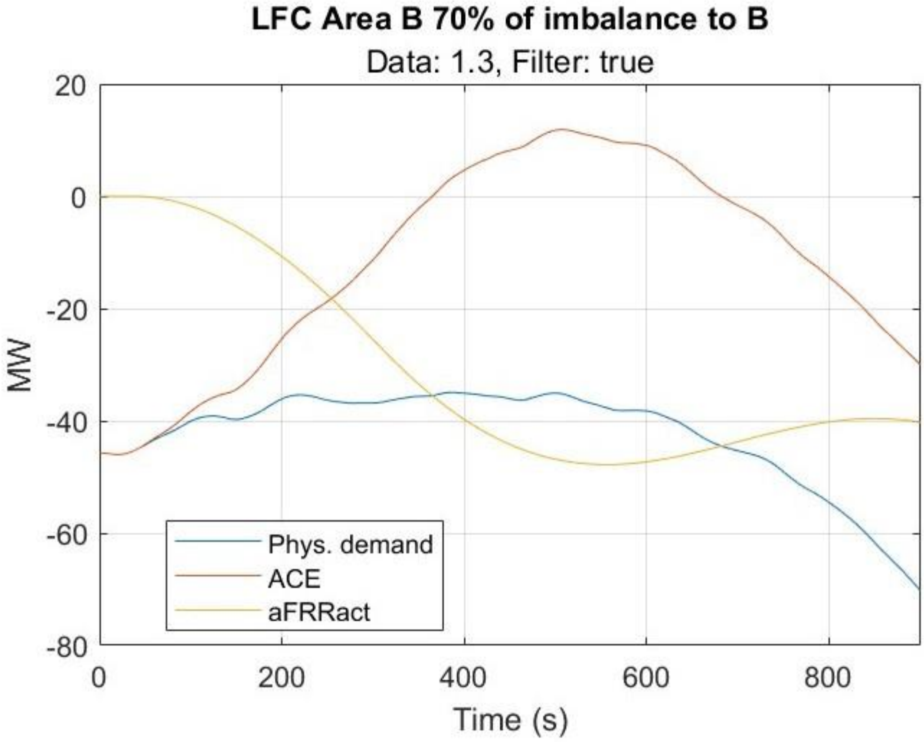


Figure 18. Alternative 3, data 1.3, filtering, LFC area B.

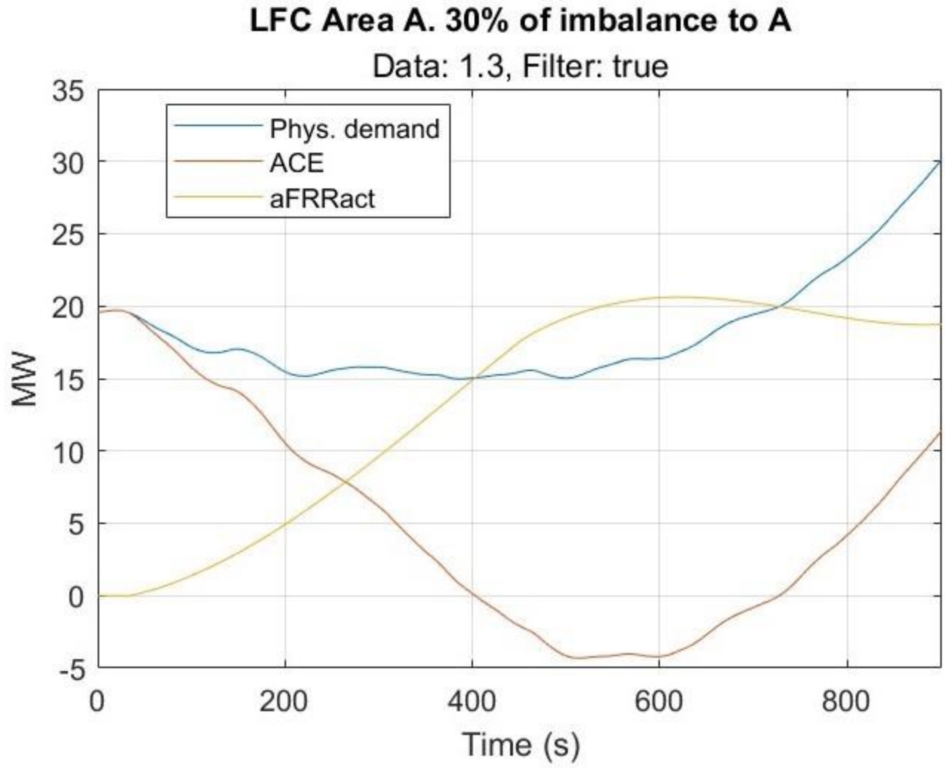


Figure 19. Alternative 3, data 1.3, filtering, LFC area A.

d

### 4.4.4 Alternative 4: Local Battery Reserve

This configuration retains all imbalances locally, representing an idealized battery control scenario. Although batteries are not physically modeled, the required storage capacity is estimated by integrating the imbalance over time to approximate the energy storage needed to fully manage imbalances on-site. The analysis focuses on the worst-case scenario using dataset 3.4 to assess the maximum storage requirements.

The battery control strategy was assessed using a simplified model focusing solely on available capacity over a 15-minute window. The results showed that a storage capacity of approximately 0.1 GWh would be sufficient to handle the filtered imbalance signal. This is technically feasible with current battery technology and aligns with commercial offshore wind farm applications.

However, the model does not consider dynamic battery behavior, including charging and discharging rates, round-trip efficiency, degradation, or state-of-charge constraints. Furthermore, the simulation only spans a short time frame; scaling the control strategy to one-hour or day-long windows would require significantly more storage, potentially into the multi-GWh range, which is not currently practical for offshore deployment.

Therefore, the battery solution appears promising for short-term, high-frequency smoothing, but it is not suitable as a stand-alone long-term balancing mechanism.

The results for the battery-based control strategy are summarized using one filtered case, which illustrates the storage requirement and smoothing effect. An additional unfiltered case is included in the Appendix.

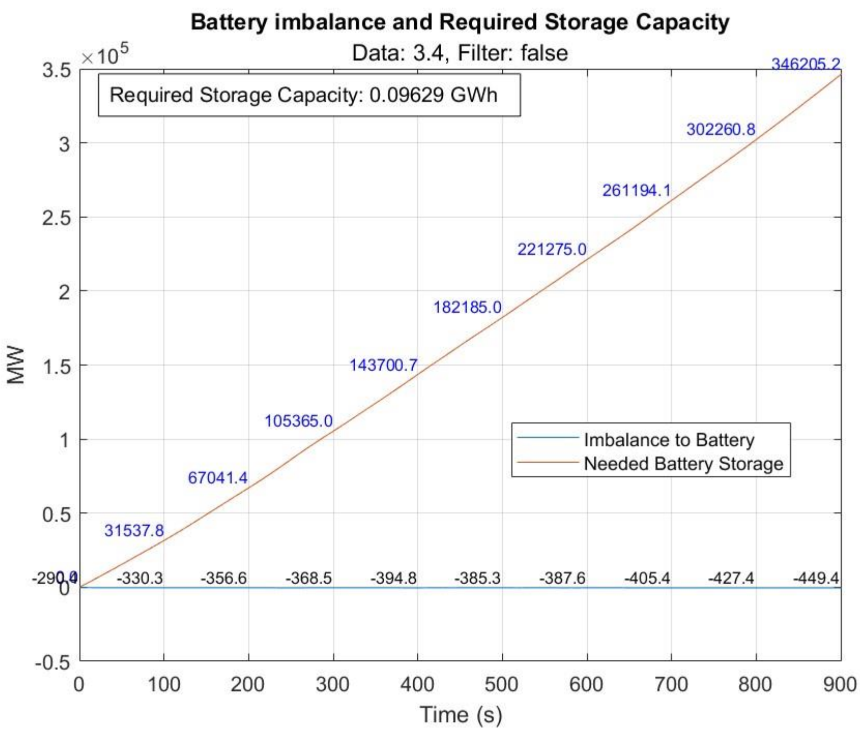


Figure 20. Alternative 4, data 3.4, no filtering

## 4.5 Summary of Control Results

Alternative 3 consistently showed the most stable system performance, when managing typical imbalances from offshore wind connected to two LFC areas. By distributing the imbalance between two LFC areas, it reduced strain on both HVDC links by balancing flows more evenly and made efficient use of available frequency restoration reserves. ACE deviations were reduced, and control actions remained within reasonable operational limits across most scenarios. Alternative 1 also showed strong performance, mainly due to the large aFRR volume available in LFC area B, though this benefit is specific to system configurations with similarly strong reserves.

Alternative 2 frequently encountered HVDC saturation and reserve shortages, particularly during overproduction cases, which resulted in sustained ACE deviations that could not be corrected. It also became clear that LFC area A would not be able to manage large imbalances even if roles were reversed with LFC area B, due to insufficient aFRR.

Alternative 4 (Battery Control) proved capable of balancing short-term filtered imbalances with modest storage requirements (~0.1 GWh). However, it lacks scalability for longer durations, and the simplified modeling omits essential dynamics such as charging limits and efficiency. Filtering consistently helped reduce ACE volatility and smoothed the control signals, but cannot address structural issues like saturated HVDC links or reserve exhaustion.

# 5 Conclusion and Future work

## 5.1 Conclusions

This thesis evaluated four different control strategies for balancing offshore wind power using HVDC links and local aFRR resources in LFC areas. The results demonstrate that balancing performance is shaped by a combination of reserve availability, HVDC transmission constraints, and control allocation strategy. Across all alternatives, Alternative 3, with the imbalance split between LFC areas, provided the most balanced and robust control performance. It effectively minimized ACE volatility while avoiding frequent link overloads. Alternative 1, where all imbalances were sent to LFC area B, also performed well, primarily due to the high aFRR reserves available in LFC area B, but may not scale without similar reserve availability. Alternative 2, where all imbalances were sent to LFC area A, struggled with persistent HVDC link A saturation and insufficient reserve capacity in LFC area A, particularly during overproduction events. Battery-based control in Alternative 4 proved effective for short-term energy smoothing, though not suitable for longer-term balancing without scaling. Furthermore, in some scenarios, even if the roles of LFC area A and LFC area B were reversed, LFC area A would still be unable to manage the imbalance effectively due to its limited aFRR capacity.

Alternative 3, which distributes the imbalance between two LFC areas, consistently delivered the most stable and robust system response, in terms of balancing the offshore wind power. Alternative 1 performed well due to the relatively large aFRR capacity in LFC area B, while Alternative 2 was limited by HVDC saturation and insufficient reserves in LFC area A. Battery-based control in Alternative 4 proved effective for short-term energy smoothing, though not suitable for longer-term balancing without scaling. Furthermore, in some scenarios, even if the roles of LFC area A and LFC area B were reversed, LFC area A would still be unable to manage the imbalance effectively due to its limited aFRR capacity.

The model does not consider netting effects between multiple TSOs, meaning the results are conservative with respect to reserve use. Additionally, while filtering improves control behavior in simulations, its feasibility and implementation in practice—particularly regarding both the speed and scale at which such filtering could be executed in real systems, especially compared to traditional physical control actions like pitch adjustments—remains uncertain.

It is also important to recognize that HVDC capacities were modeled to match maximum production. In real-world applications, oversizing HVDC links could provide beneficial headroom for absorbing surplus energy and handling imbalances more flexibly. This is especially relevant when considering the scaling of the model to multiple wind farms and interconnected offshore platforms, which will be essential components of the future European offshore grid.

## 5.2 Recommendations for Future Work

Future research should begin by scaling the model to include multiple HVDC links and coordinated control zones, enabling analysis of complex scenarios involving several offshore wind farms and their interactions.

To further improve realism, future studies should also consider incorporating normal imbalances within the LFC areas, rather than initializing simulations at a perfectly balanced 50 Hz. This would provide a more representative starting point and help assess control strategies under realistic system conditions. Additionally, relevant HVDC system constraints—such as zero-crossing limitations—should be modeled to reflect physical operational boundaries. Including balancing markets such as mFRR would also allow for analysis of reserve activation coordination and its effect on system stability.

Integrating the model into larger frameworks involving multiple TSOs and interconnected grid networks would capture the complexities of cross-border coordination and its effects on imbalance management and system stability in increasingly interconnected power systems.

The application of a more advanced control system is suggested to enable dynamic optimization of system efficiency and resource utilization in real time.

Simulation periods should be extended to full-hour and multi-hour durations to better evaluate long-term system behavior, including battery recharging strategies and the cumulative impact on operational reliability and asset health.

Further development of wind farm models is recommended, incorporating features such as droop control, synthetic inertia, and fast local frequency support, to improve the accuracy and realism of simulations. Additionally, the feasibility and practical implementation of filtering techniques within control systems should be further investigated.

Improved battery modeling—covering charging and discharging logic, state of charge tracking, efficiency losses, and degradation mechanisms—would enhance the ability to predict battery performance and lifespan.

# 6 References

[1] ENTSO-E, "TYNDP 2024 Sea-Basin ONDP Report: TEN-E Offshore Priority Corridor: Northern Seas Offshore Grids," ENTSO-E, Brussels, 2024.

[2] Svenska Kraftnät, "Balancing market outlook 2030," 19 December 2024. [Online]. Available: https://www.svk.se/siteassets/om-oss/rapporter/2024/svenska-kraftnat-balancing-market-outlook-2030.pdf. [Accessed 18 February 2025].

[3] ENTSO-E, "Offshore Network Development Plan – Roadmap 2025," ENTSO-E, Brussels, 2025.

[4] ENTSO-E, "Network Code on Load-Frequency Control and Reserves," ENTSO-E, 2013.

[5] ENTSO-E, "Operation Handbook: Policy 1 - Load-Frequency Control and Performance," Entrso-E, 2009.

[6] K. Tokumitsu, H. Amano, K. Kawabe and T. Nanahara, "Analysis and improvement of cross-regional cooperation for automatic frequency restoration reserves," *Electric Power Systems Research,* vol. 188, 2020.

[7] J. F. Manwell, J. G. McGovan and A. L. Rogers, Wind energy explained: theory, design and application, 2nd ed., Chichester: Wiley, 2009.

[8] Elia Transmission Belgium, "Explanatory Note on Elia's LFC Block Operational Agreement," Elia Transmission Belgium, 2022.

[9] ENTSO-E, "Policy on Load-Frequency Control and Reserves," ENTSO-E, 2012.

# Appendix

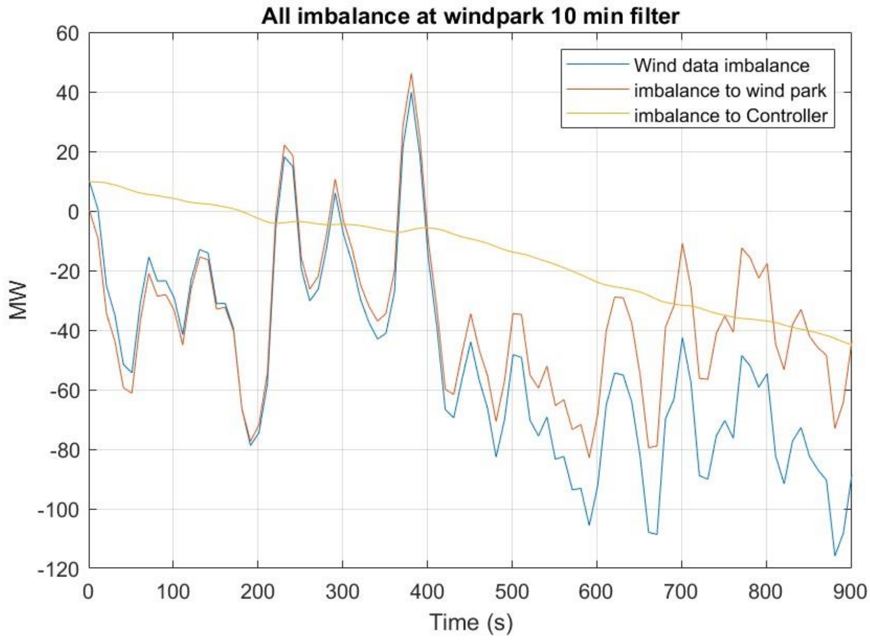


Figure 21. Ten-minute imbalance split.

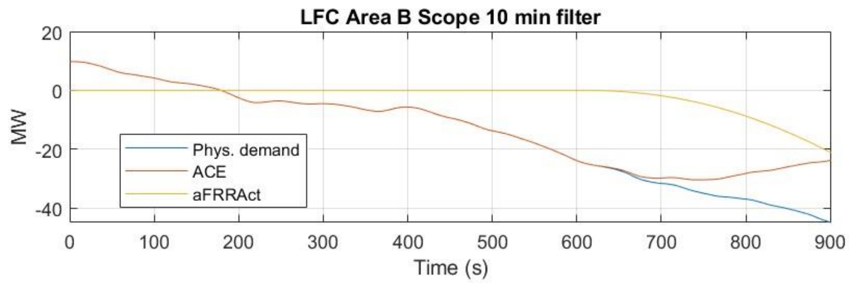


Figure 22. Ten-minute imbalance at the LFC area.

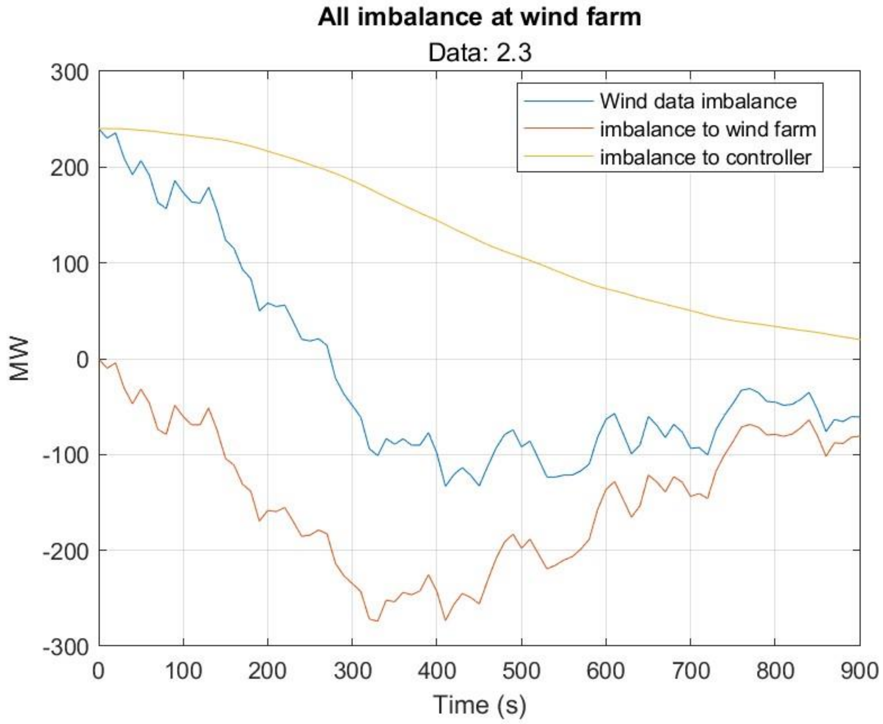


Figure 23. Filtered data 2.3.

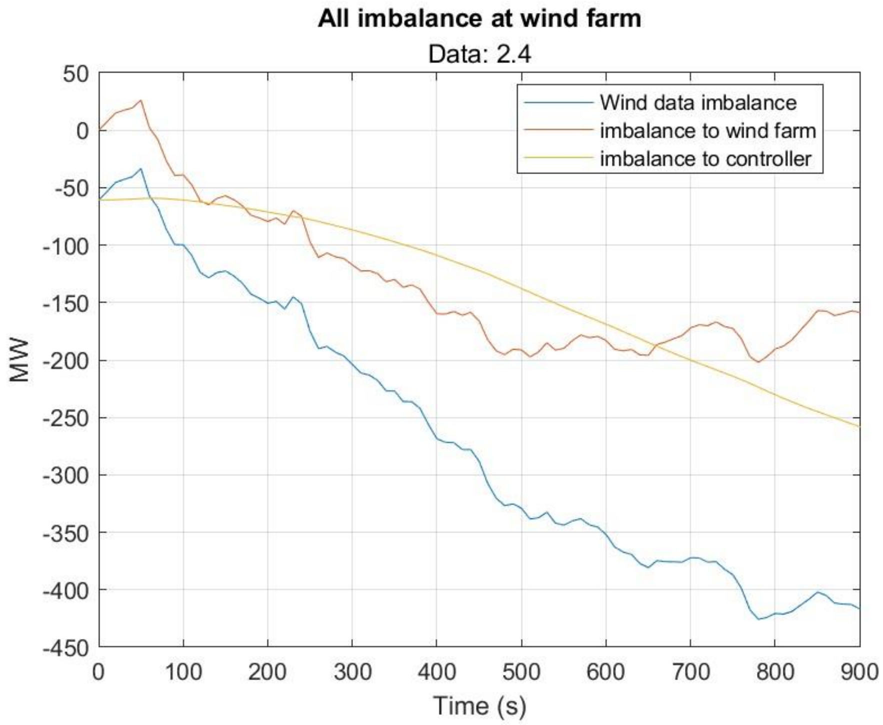


Figure 24. Filtered data 2.4.

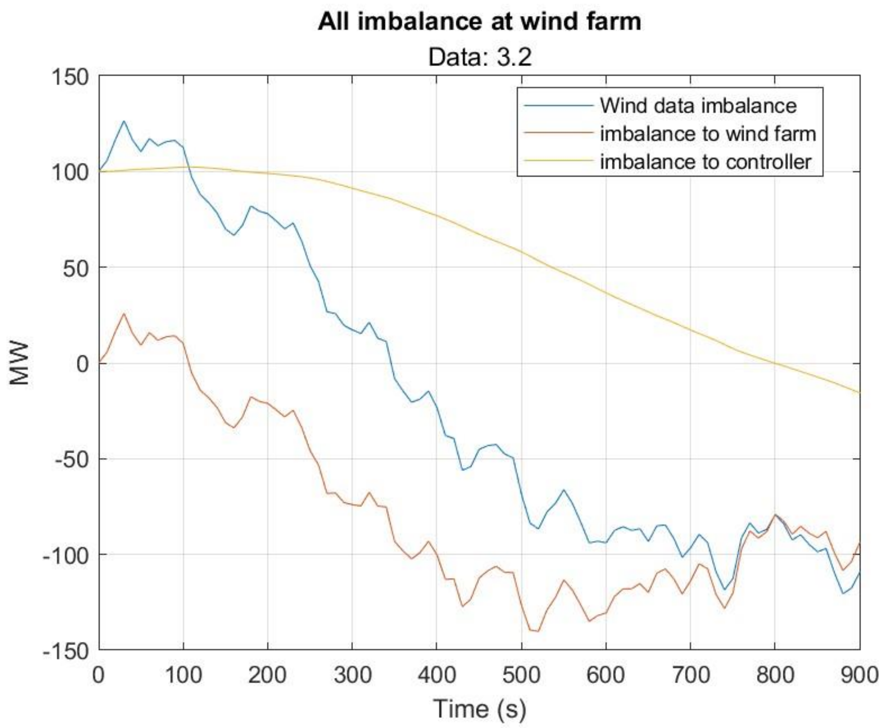


Figure 25. Filtered data 3.2.

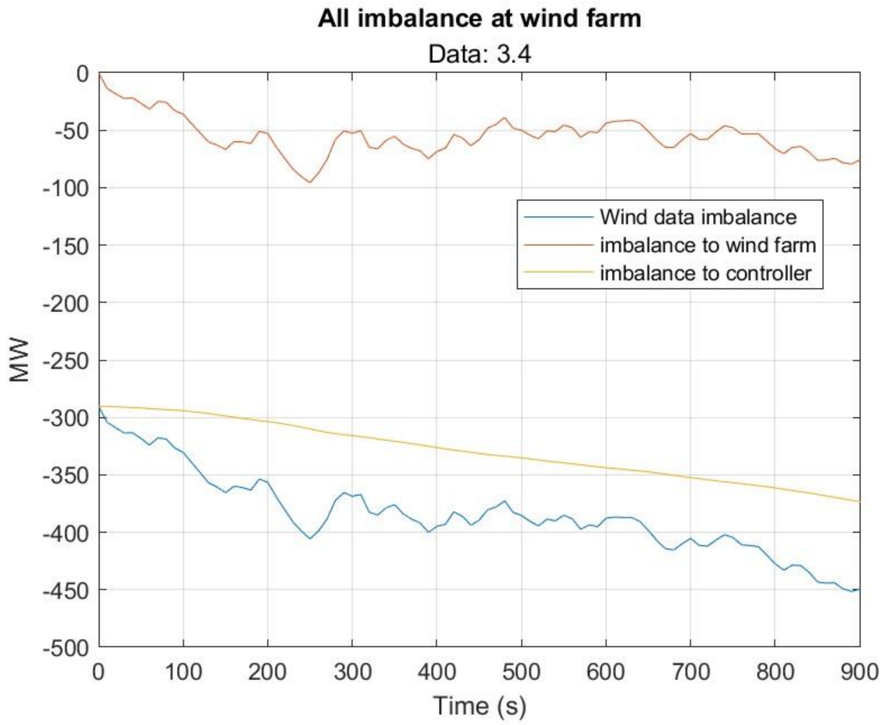


Figure 26. Filtered data 3.4.

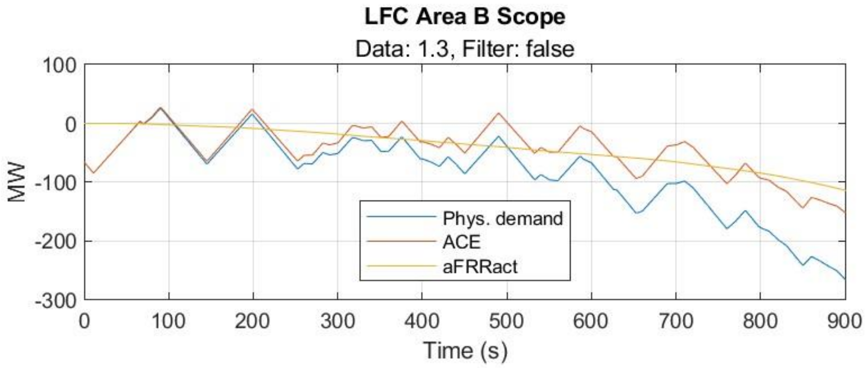


Figure 27. Alternative 1, data 1.3, no filtering, LFC area B.

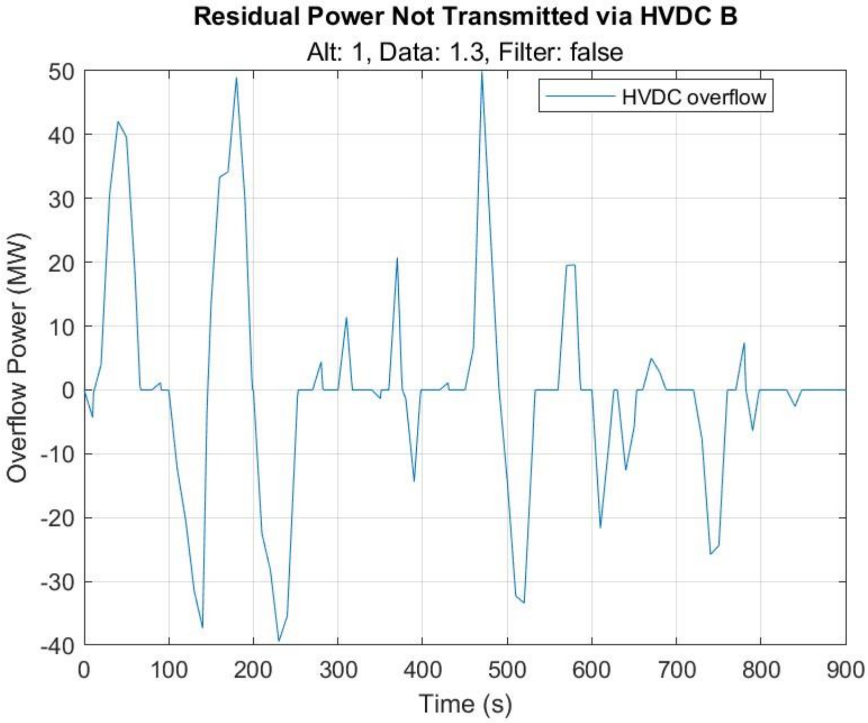


Figure 28. Alternative 1, data 1.3, no filtering, residual power.

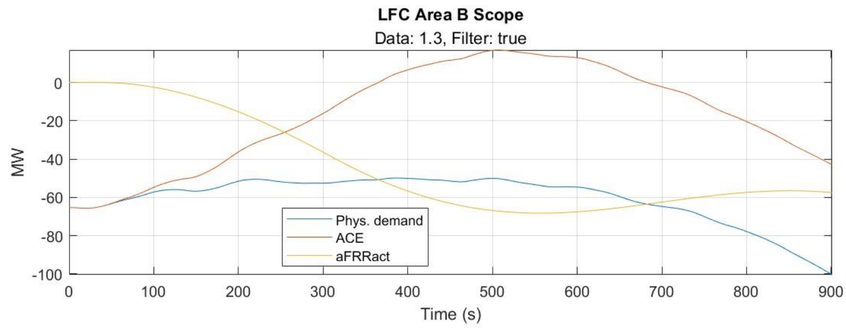


Figure 29. Alternative 1, data 1.3, filtering, LFC area B.

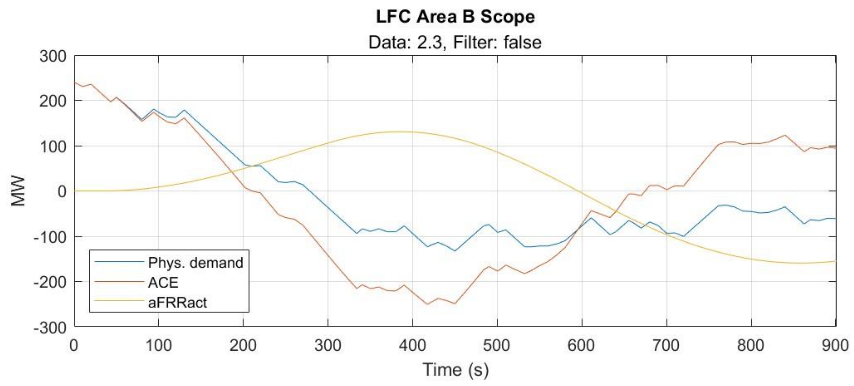


Figure 30. Alternative 1, data 2.3, no filtering, LFC area B.

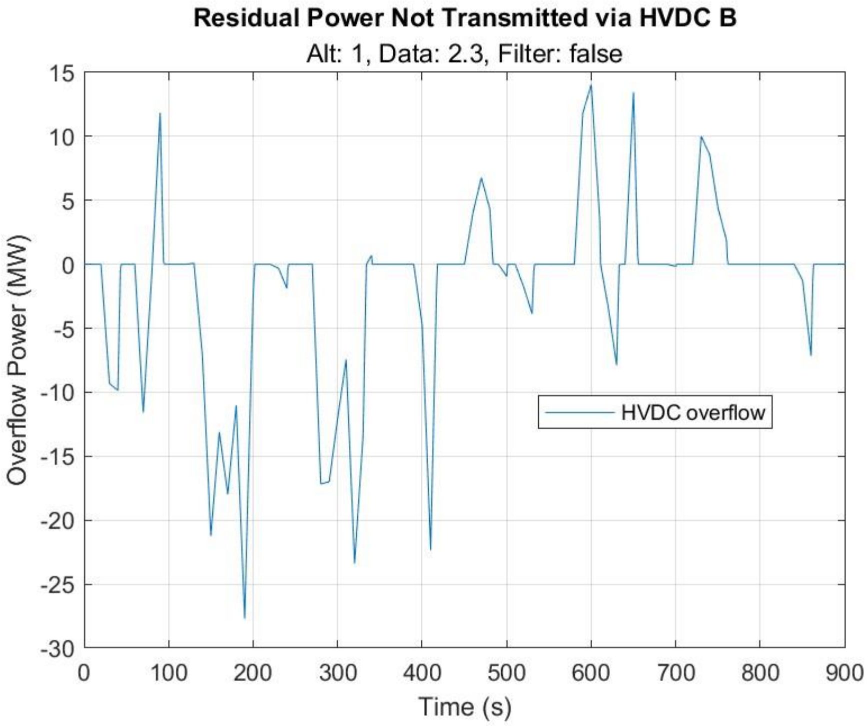


Figure 31. Alternative 1, data 2.3, no filtering, residual power.

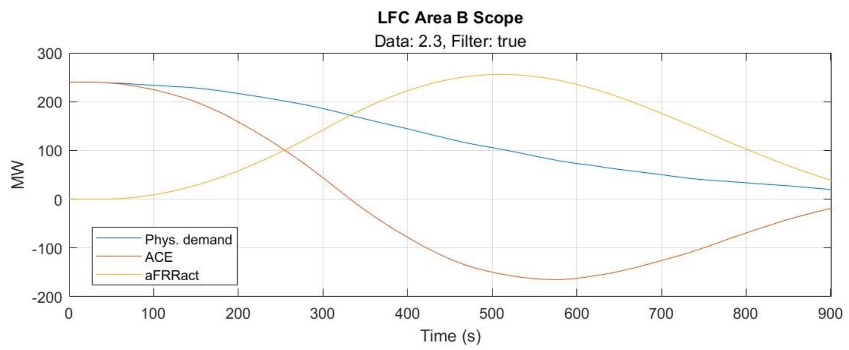


Figure 32. Alternative 1, data 2.3, filtering, LFC area B.

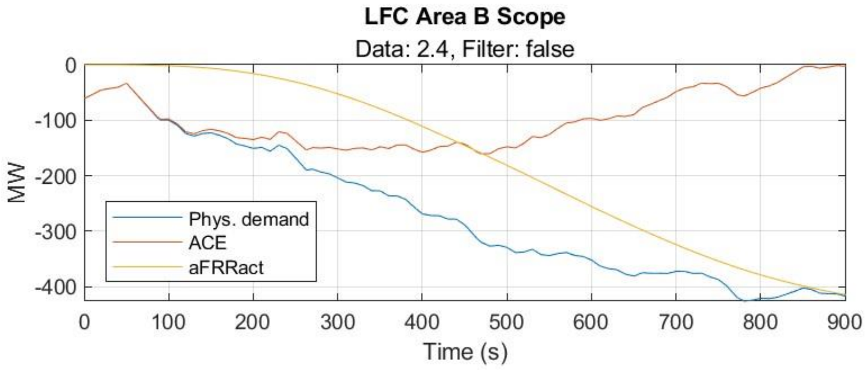


Figure 33. Alternative 1, data 2.4, no filtering, LFC area B.

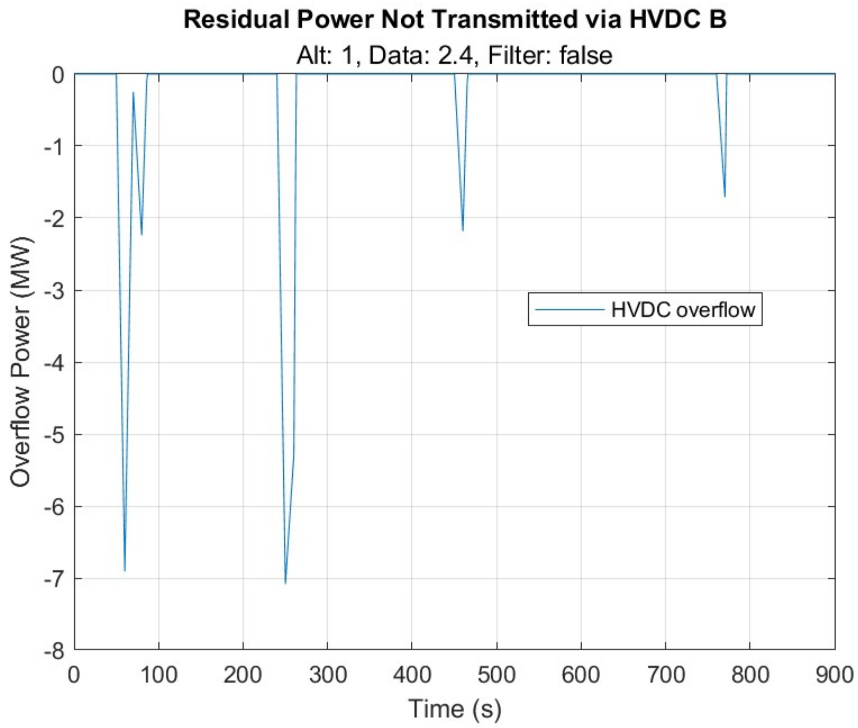


Figure 34. Alternative 1, data 2.4, no filtering, residual power.

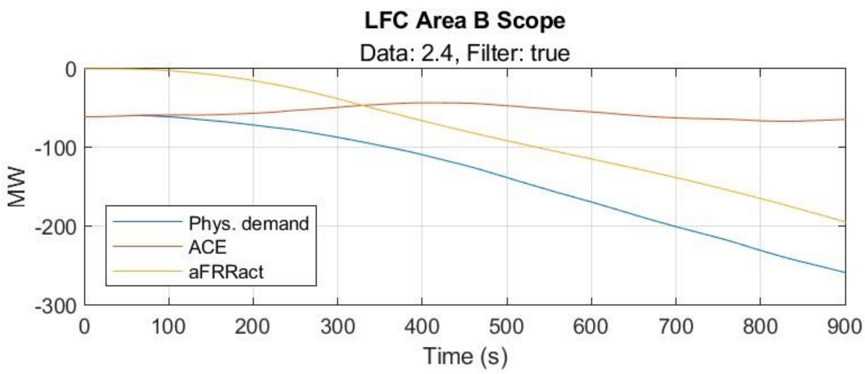


Figure 35. Alternative 1, data 2.4, filtering, LFC area B.

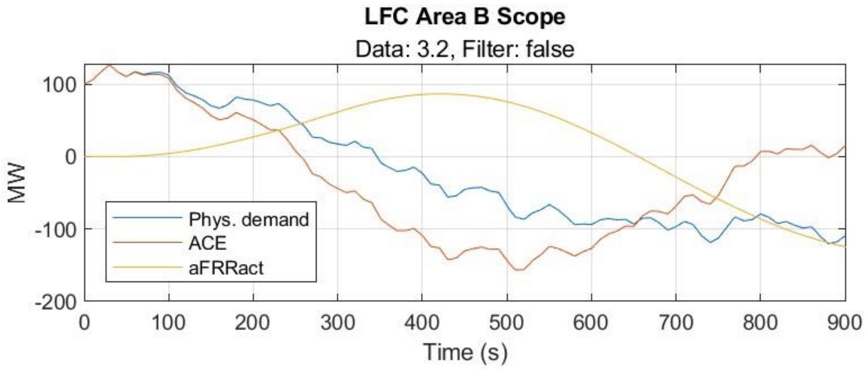


Figure 36. Alternative 1, data 3.2, no filtering, LFC area B.

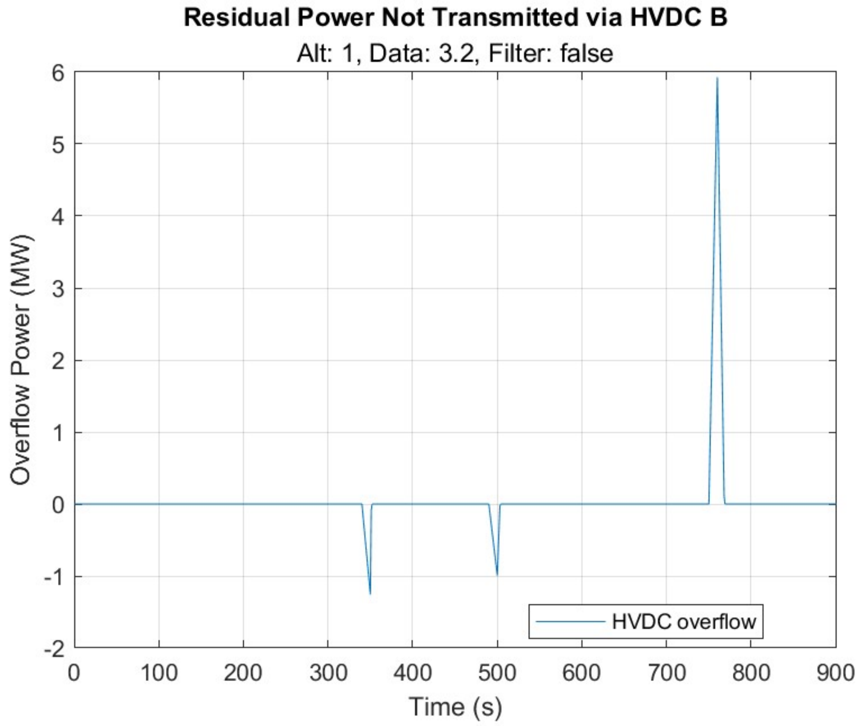


Figure 37. Alternative 1, data 3.2, no filtering, residual power.

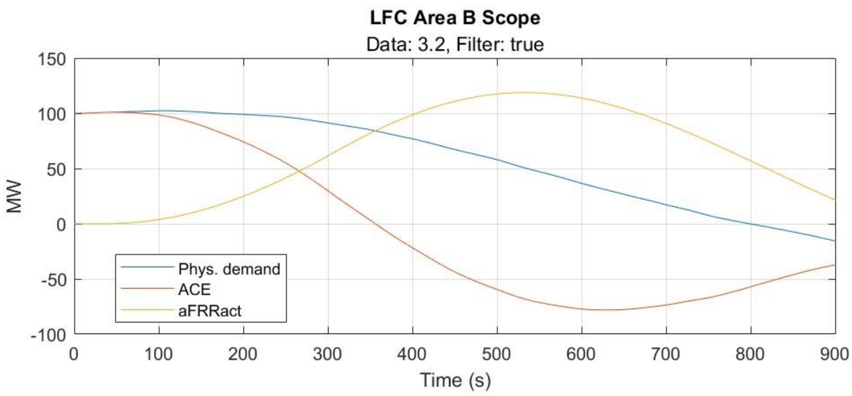


Figure 38. Alternative 1, data 3.2, filtering, LFC area B.

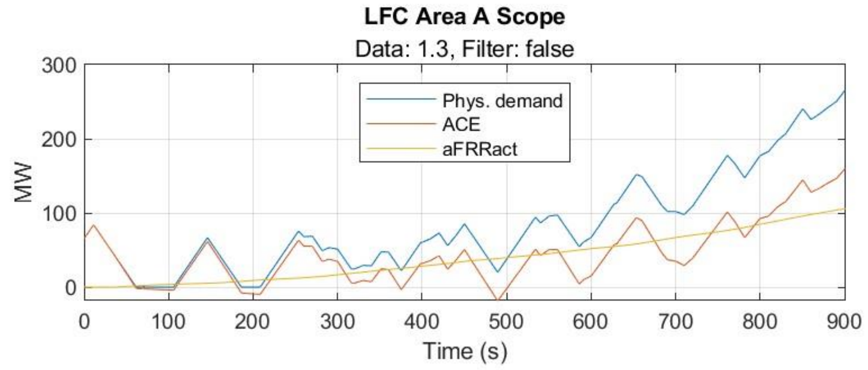


Figure 39. Alternative 2, data 1.3, no filtering, LFC area A.

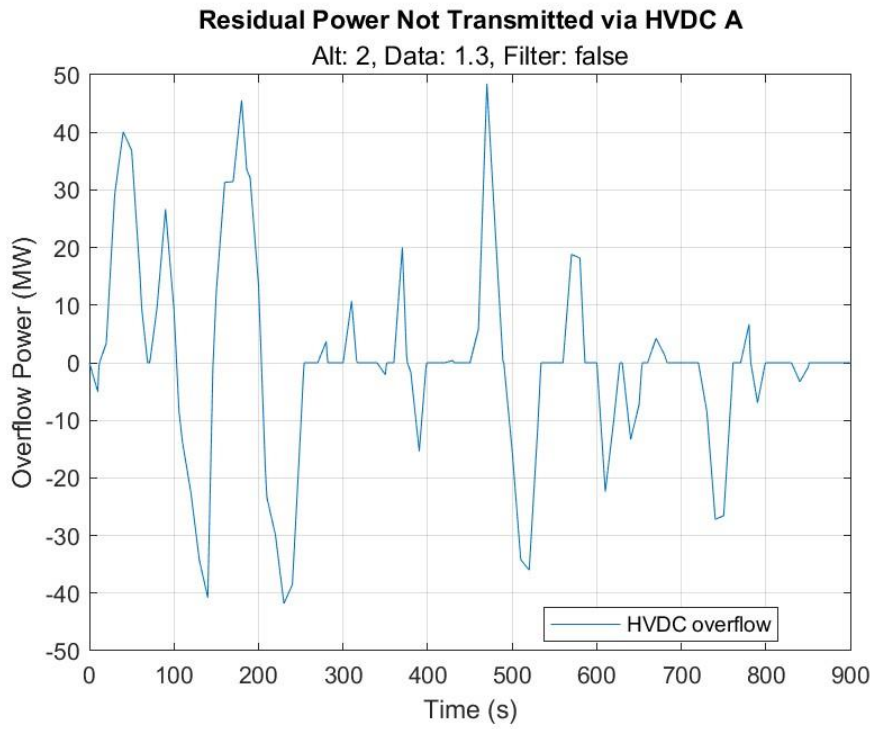


Figure 40. Alternative 2, data 1.3, no filtering, residual power.

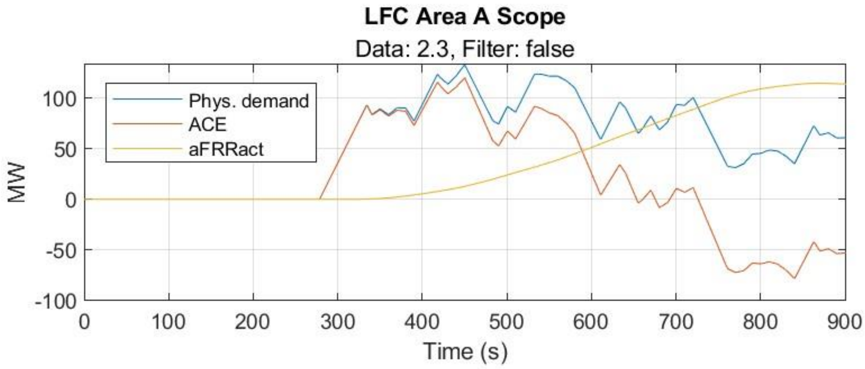


Figure 41. Alternative 2, data 2.3, no filtering, LFC area A.

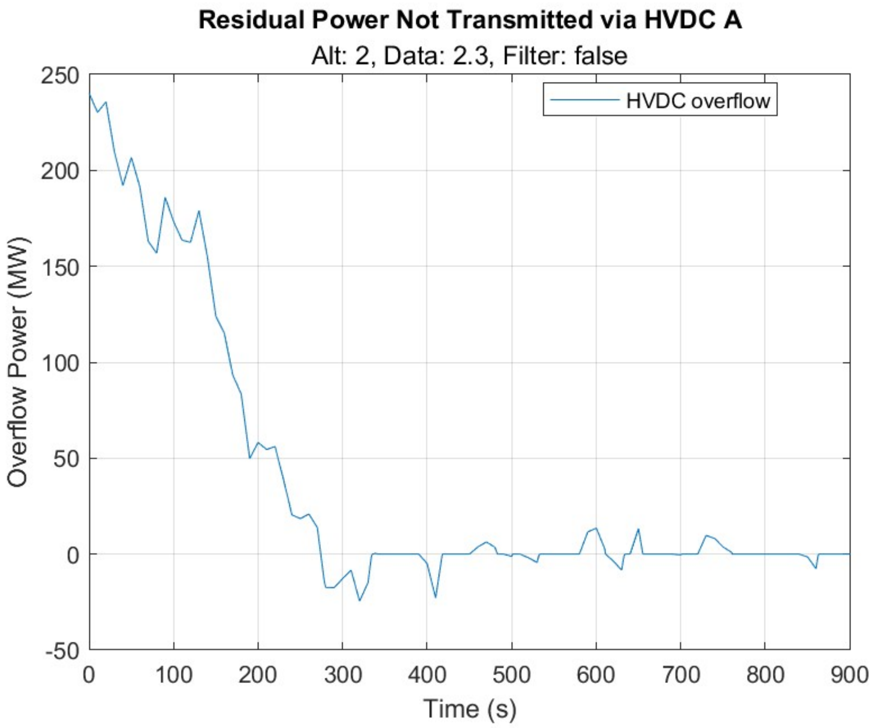


Figure 42. Alternative 2, data 2.3, no filtering, residual power

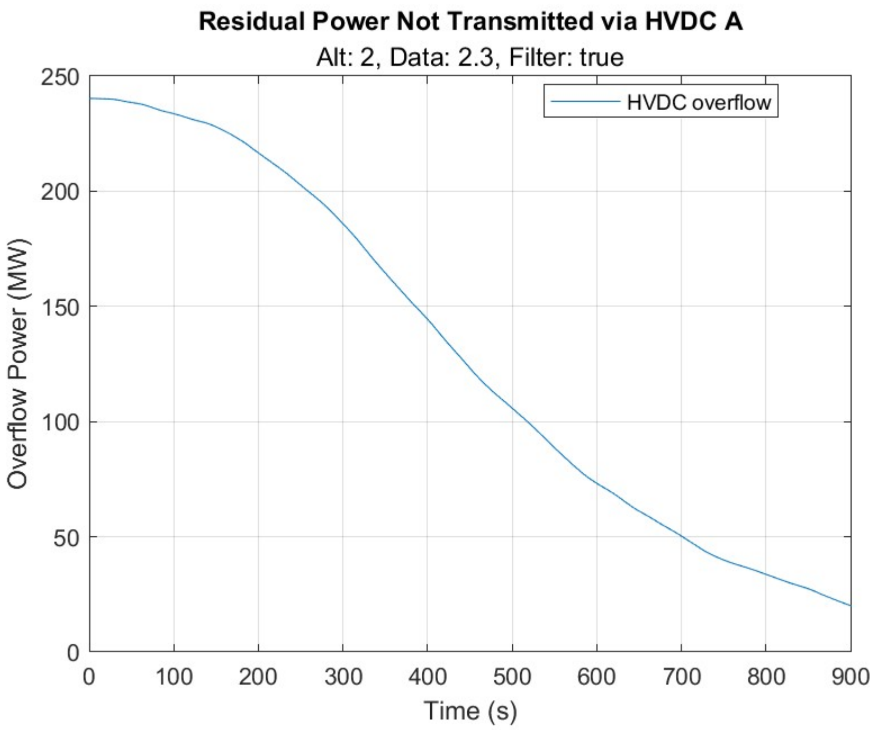

Figure 43. Alternative 2, data 2.3, filtering, residual power.

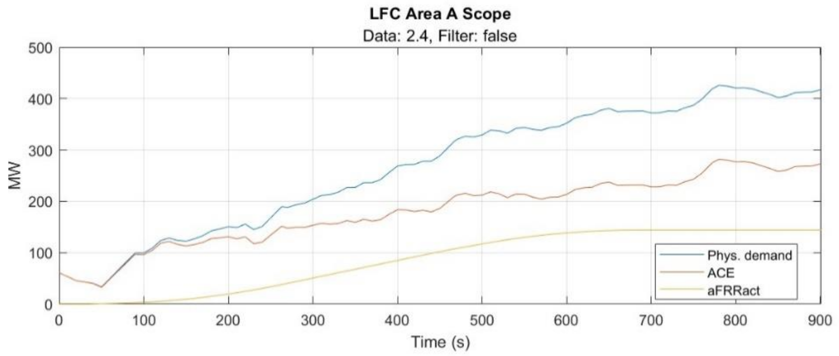


Figure 44. Alternative 2, data 2.4, no filtering, LFC area A.

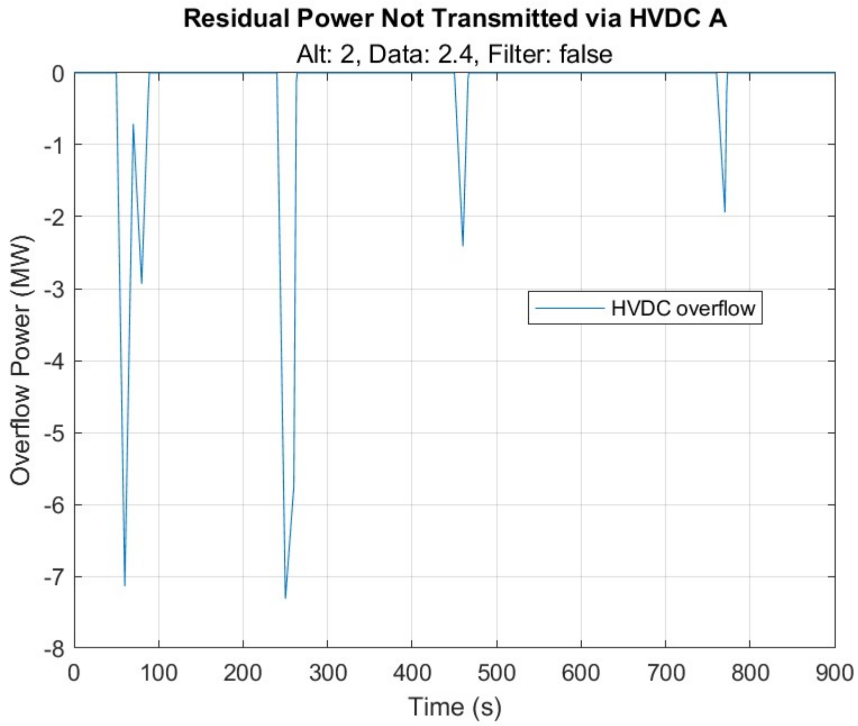


Figure 45. Alternative 2, data 2.4, no filtering, residual power.

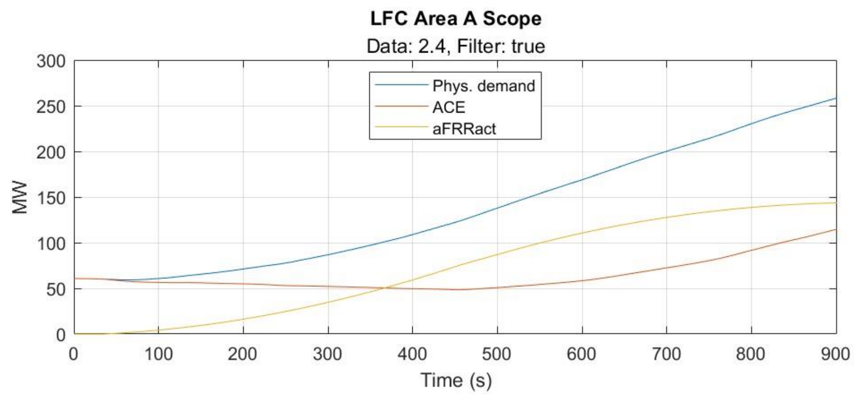


Figure 46. Alternative 2, data 2.4, filtering, LFC area A.

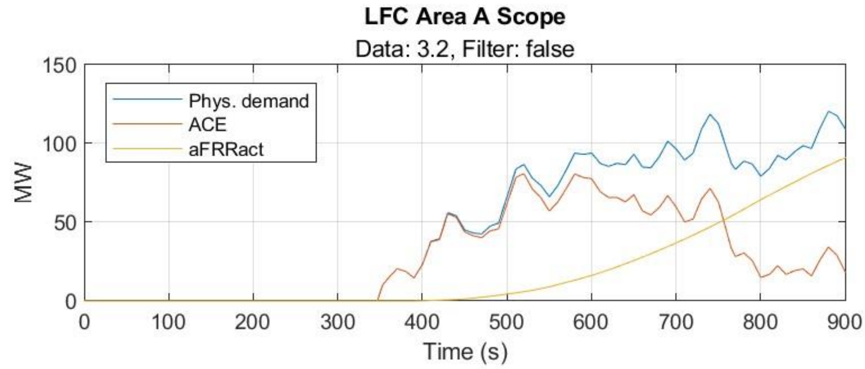


Figure 47. Alternative 2, data 3.2, no filtering, LFC area A.

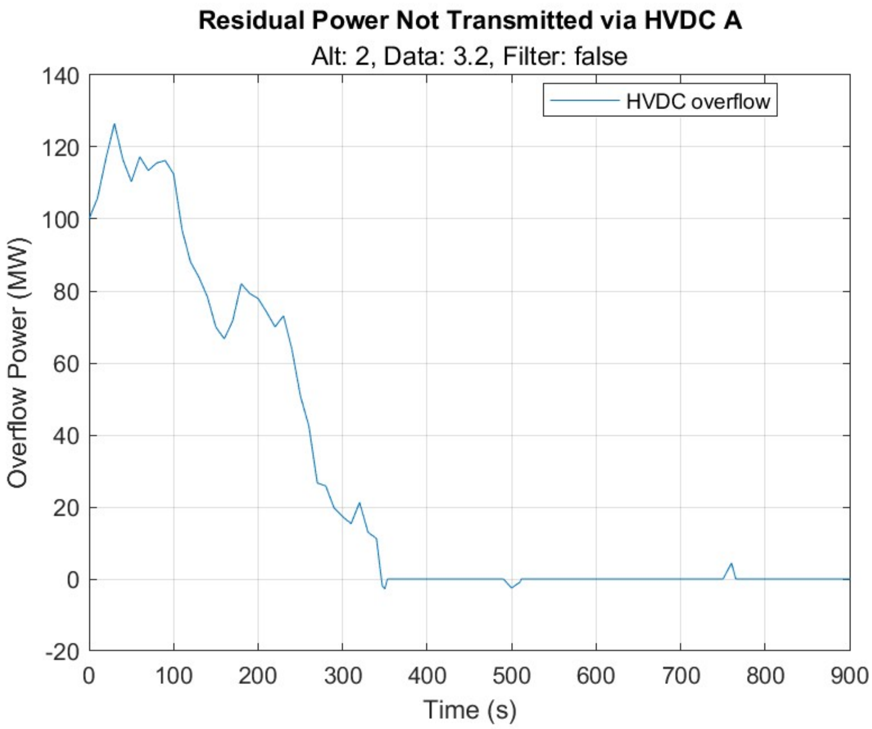


Figure 48. Alternative 2, data 3.2, no filtering, residual power.

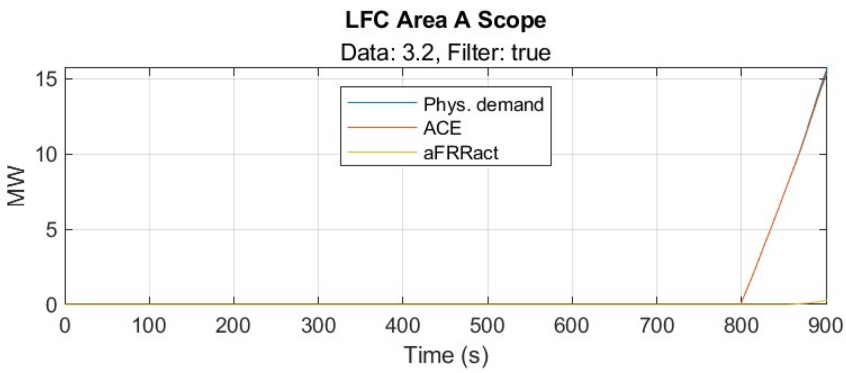


Figure 49. Alternative 2, data 3.2, filtering, LFC area A.

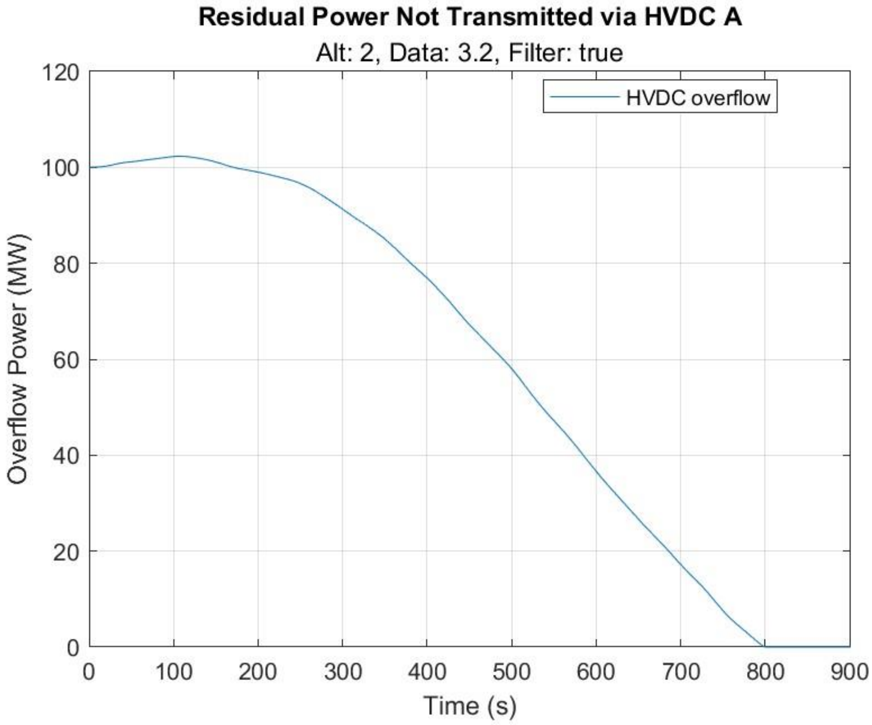


Figure 50. Alternative 2, data 3.2, filtering, LFC area A.

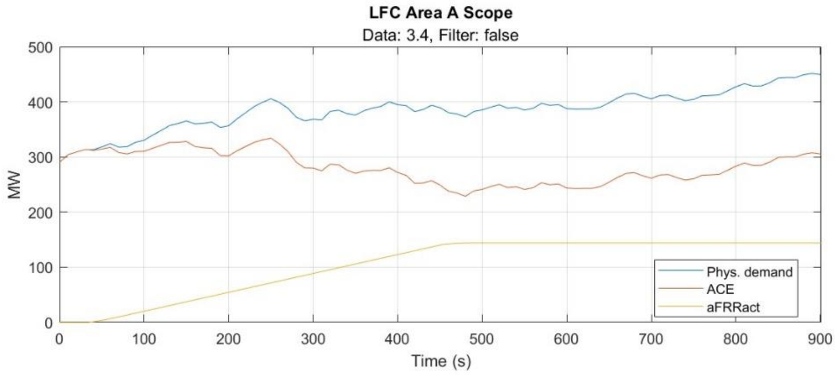


Figure 51. Alternative 2, data 3.4, no filtering, LFC area A.

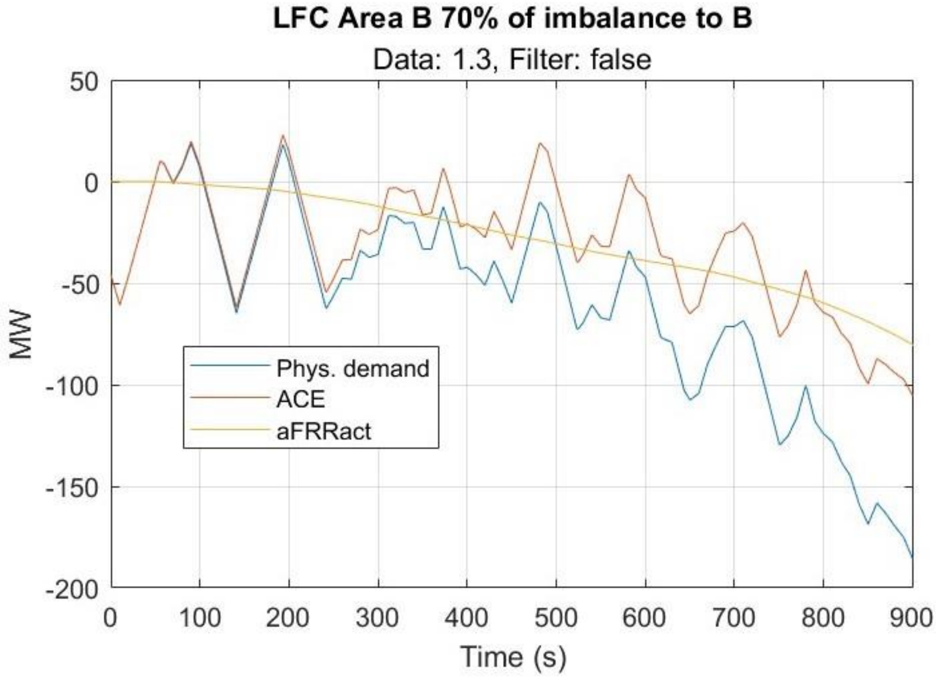


Figure 52. Alternative 3, data 1.3, no filtering, LFC B.

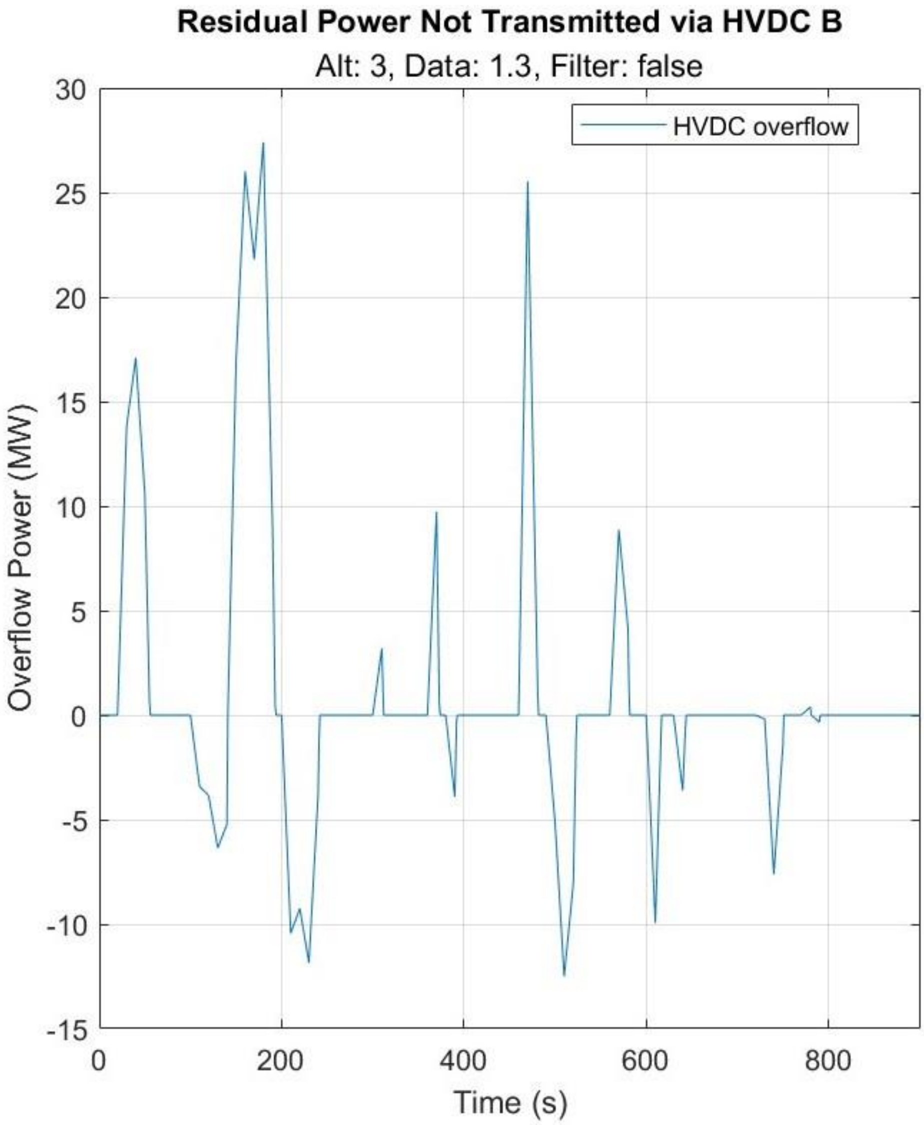


Figure 53. Alternative 3, data 1.3, no filtering, residual power not transmitted to LFC area B.

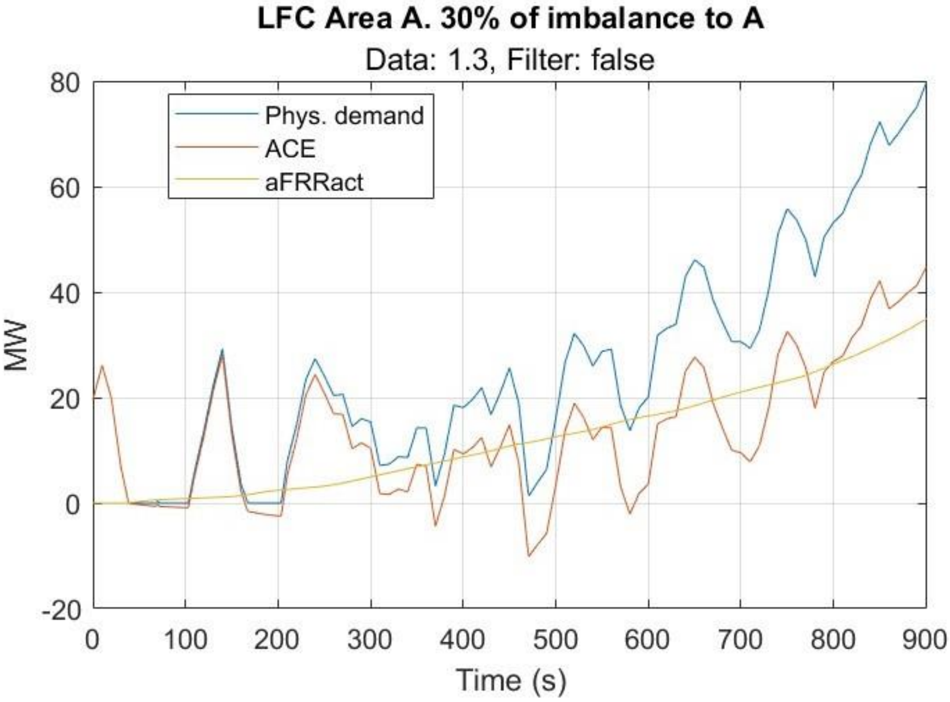


Figure 54. Alternative 3, data 1.3, no filtering, LFC area A.

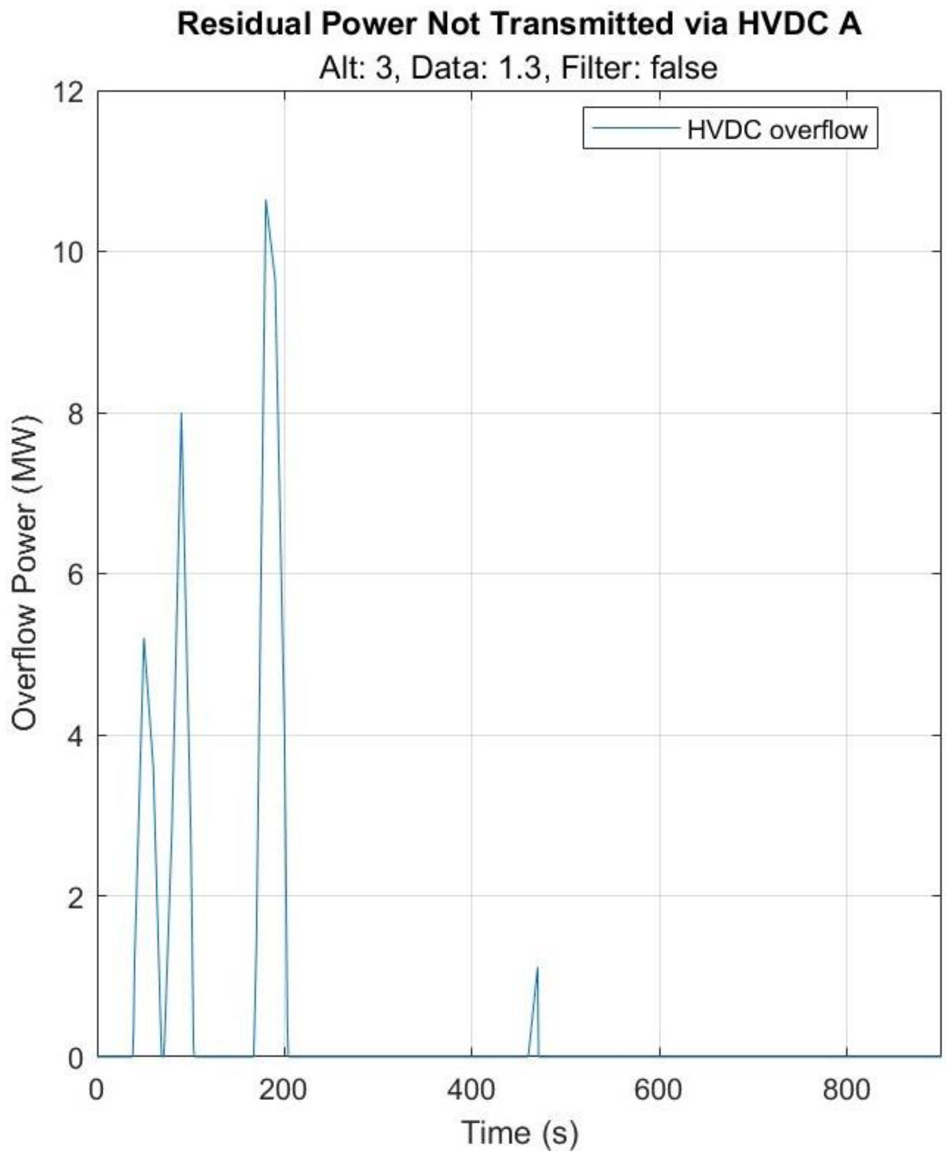


Figure 55. Alternative 3, data 1.3, no filtering, residual power not transmitted to LFC area A.

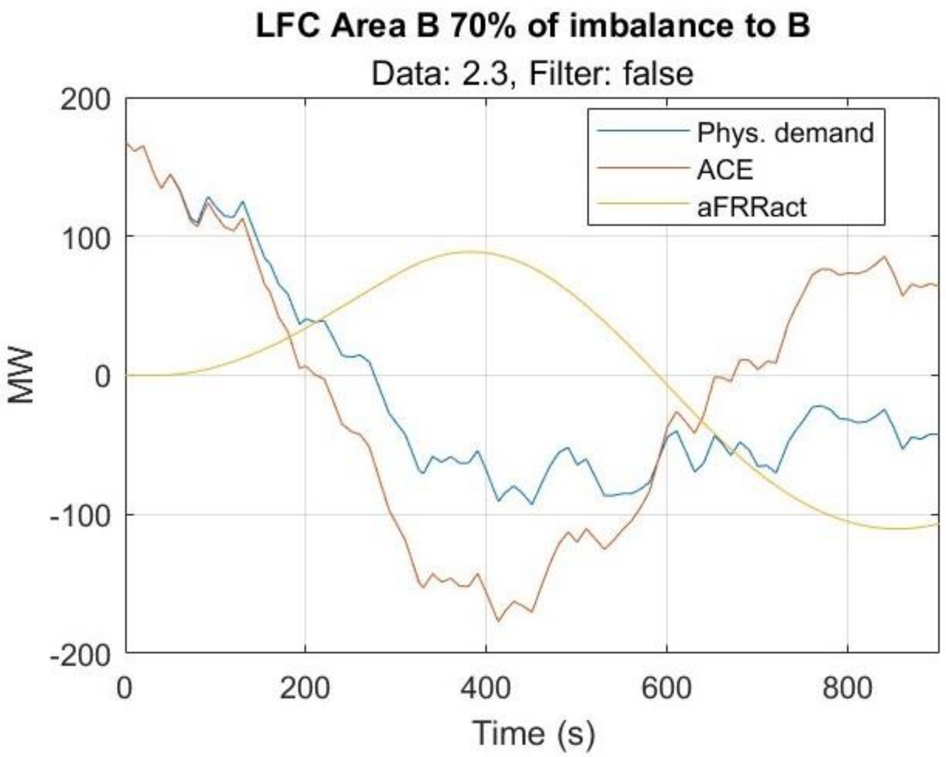


Figure 56. Alternative 3, data 2.3, no filtering, LFC area B.

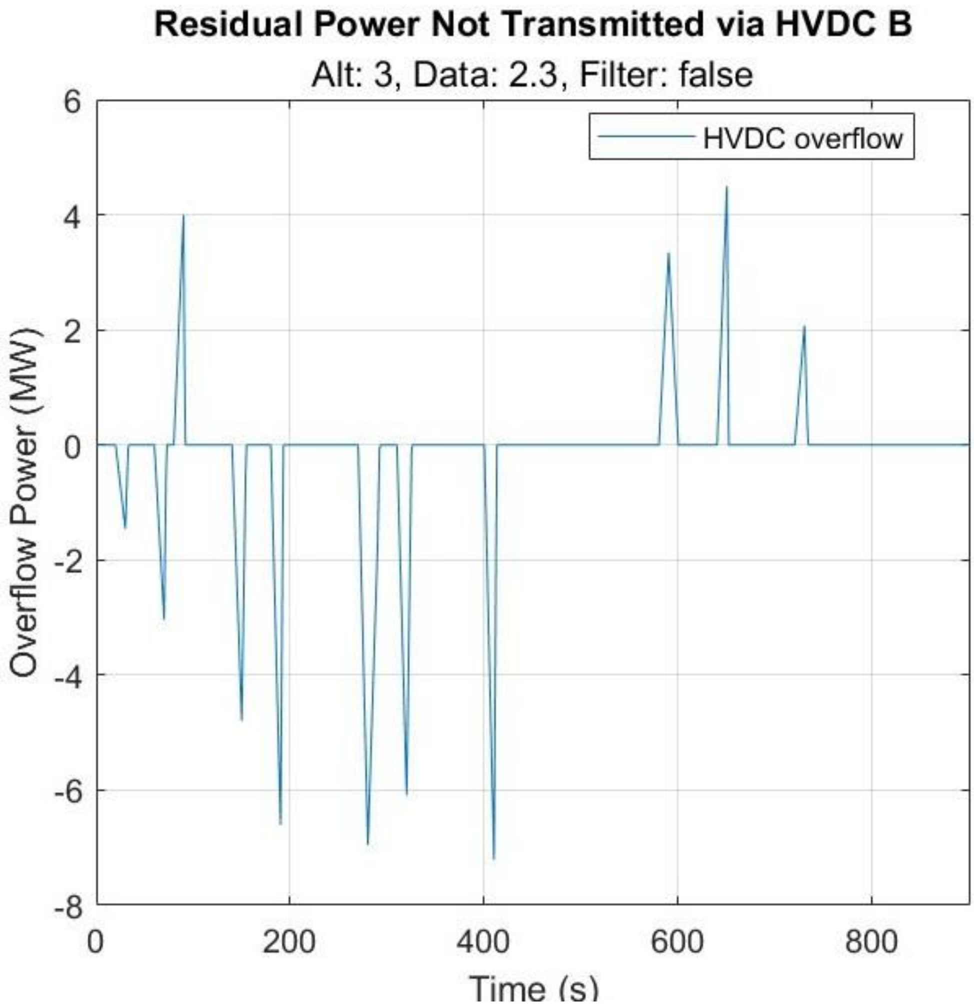


Figure 57. Alternative 3, data 2.3, no filtering, residual power not transmitted to LFC area B.

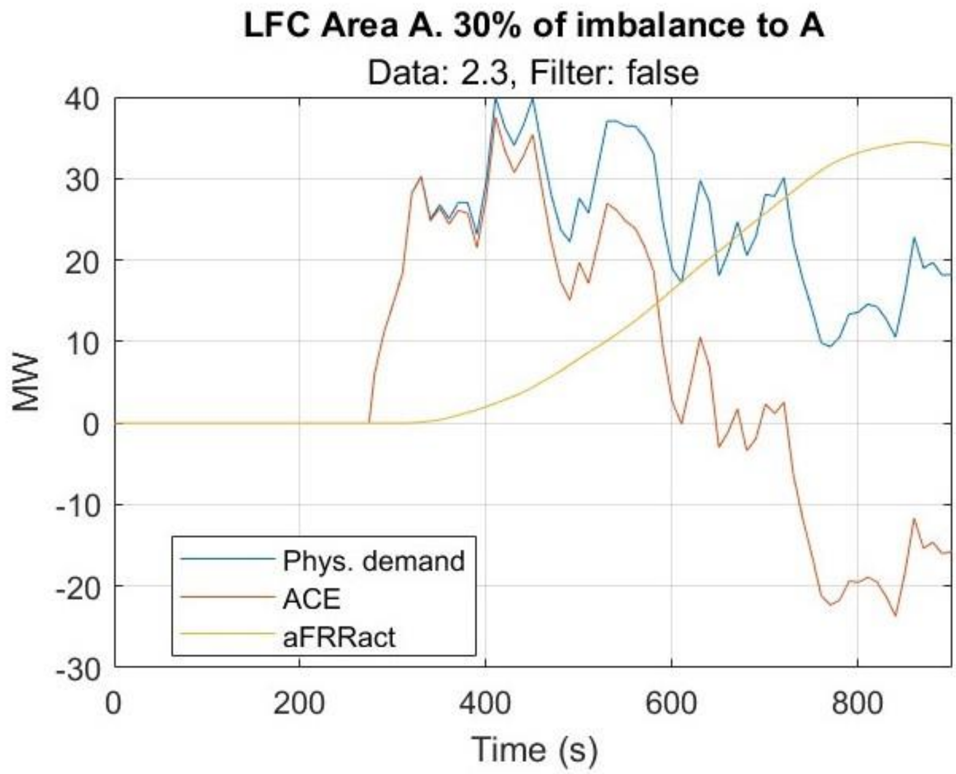


Figure 58. Alternative 3, data 2.3, no filtering, LFC area A.

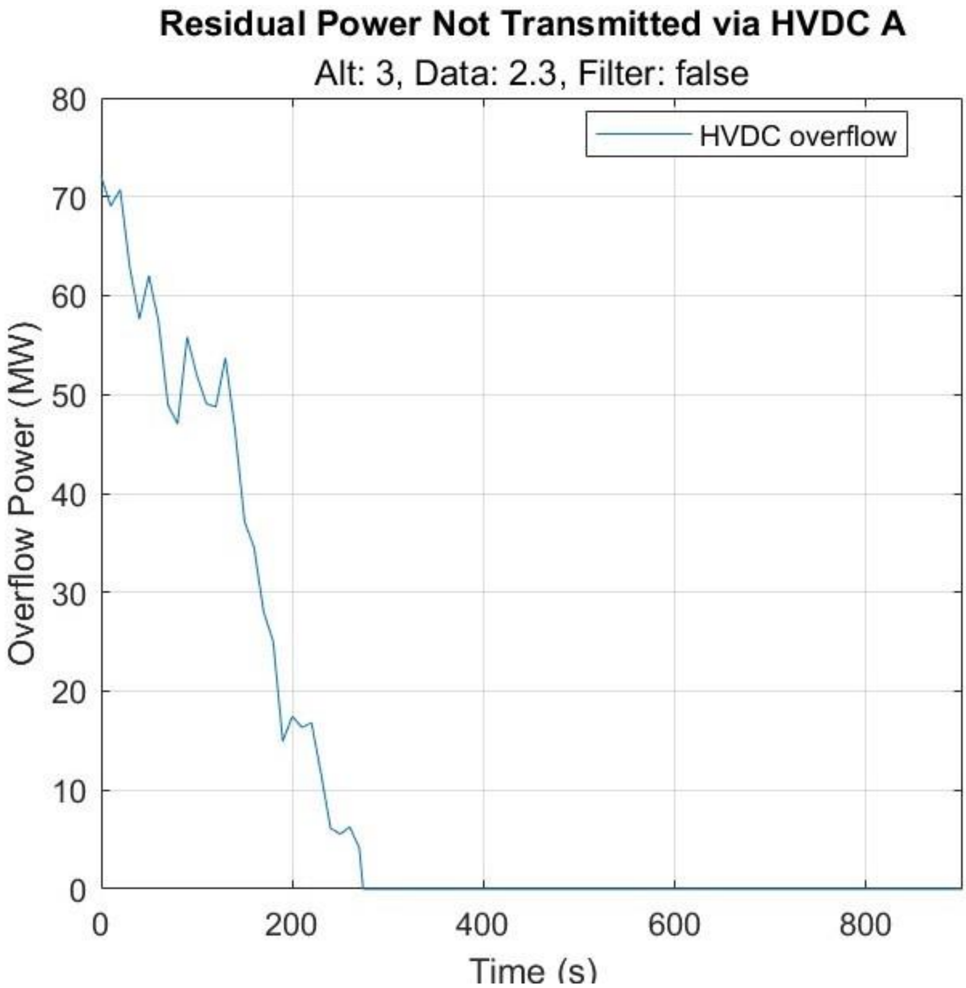


Figure 59. Alternative 3, data 2.3, no filtering, residual power not transmitted to LFC area A.

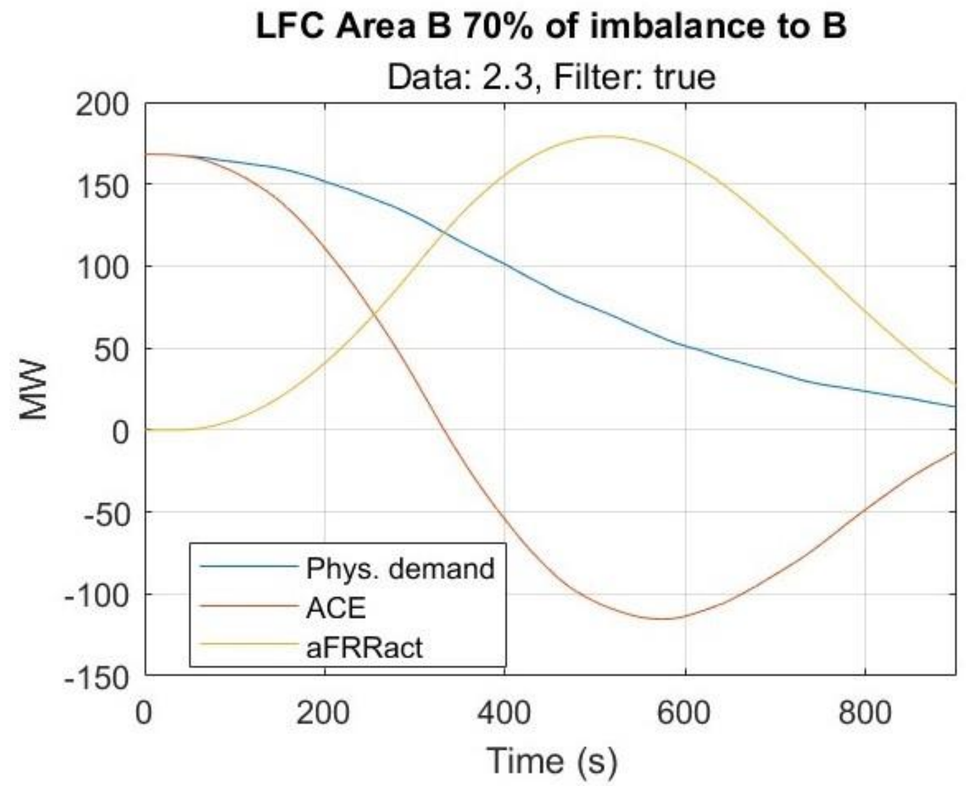


Figure 60. Alternative 3, data 2.3, filtering, LFC area B.

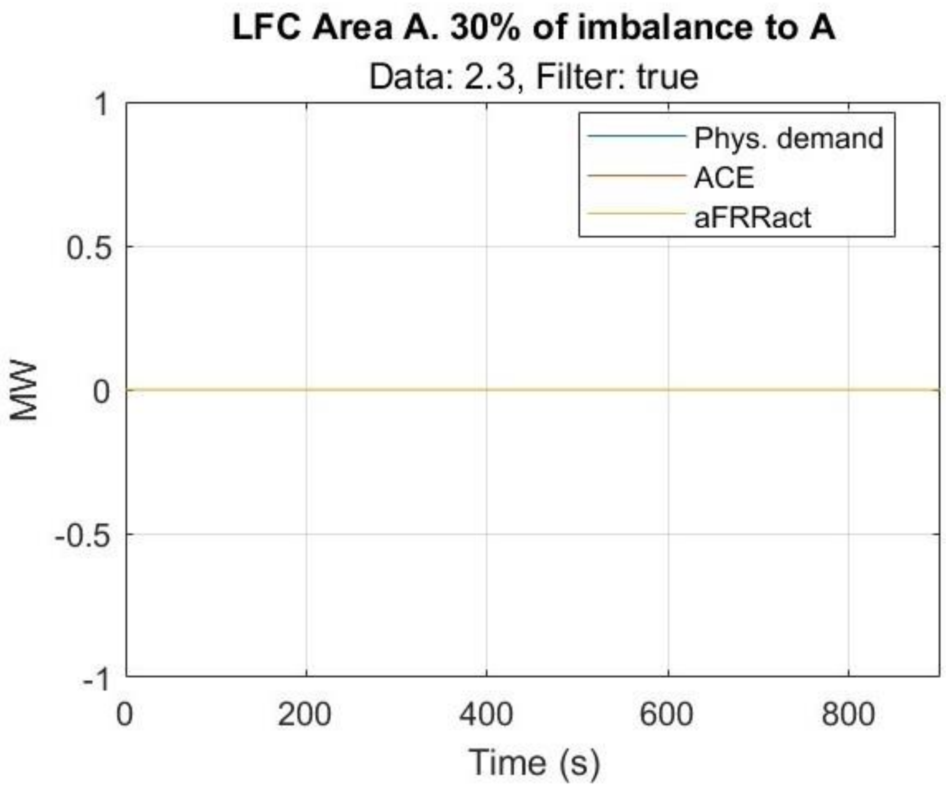


Figure 61. Alternative 3, data 2.3, filtering, LFC area A.

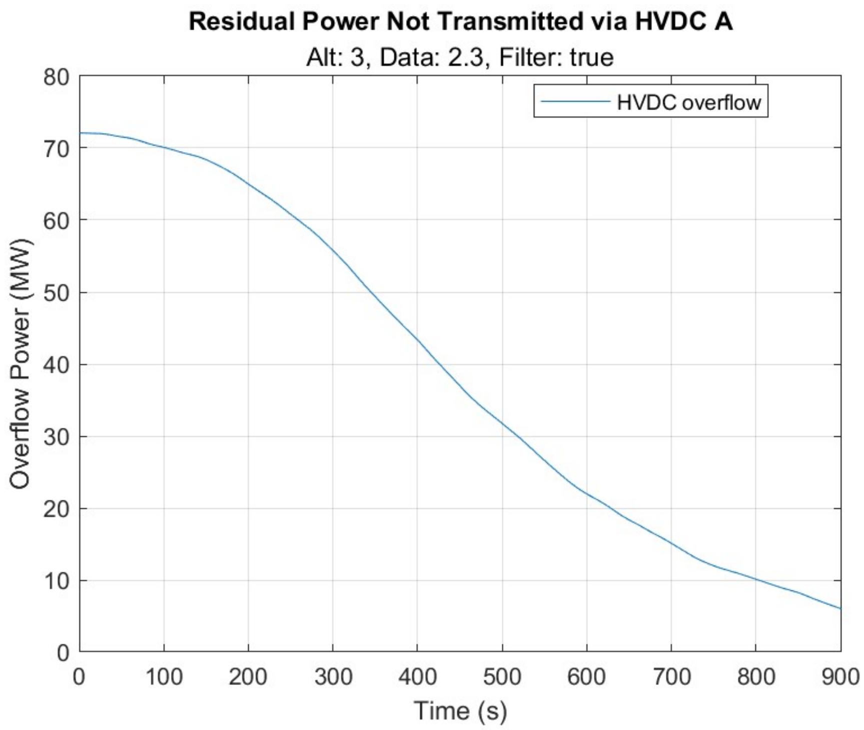


Figure 62. Alternative 3, data 2.3, filtering, residual power not transmitted to LFC area A.

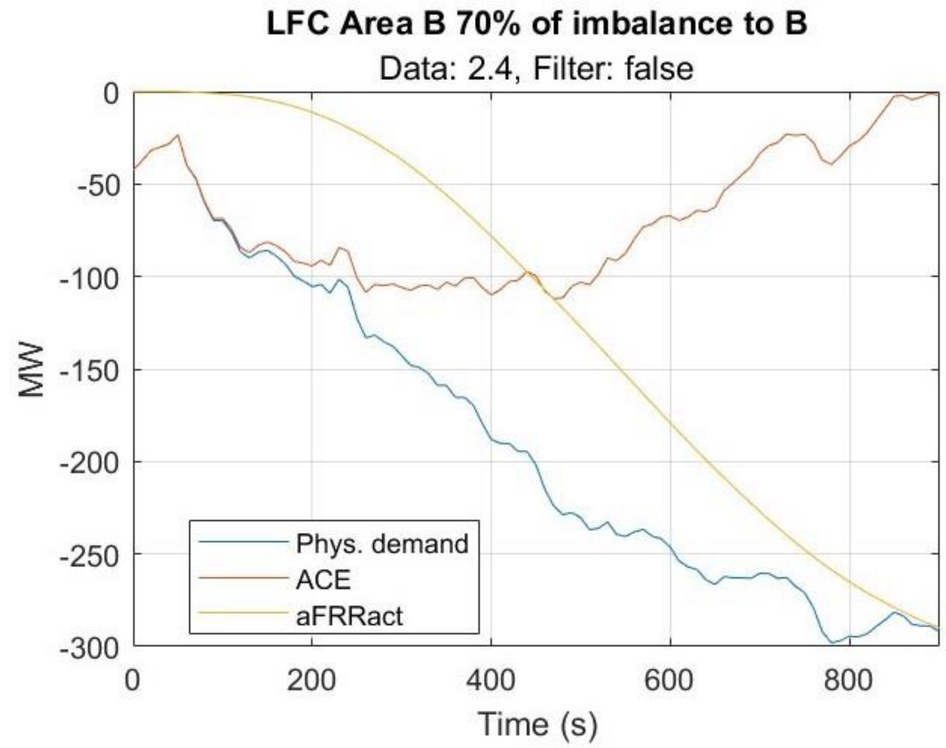


Figure 63. Alternative 3, data 2.4, no filtering, LFC area B.

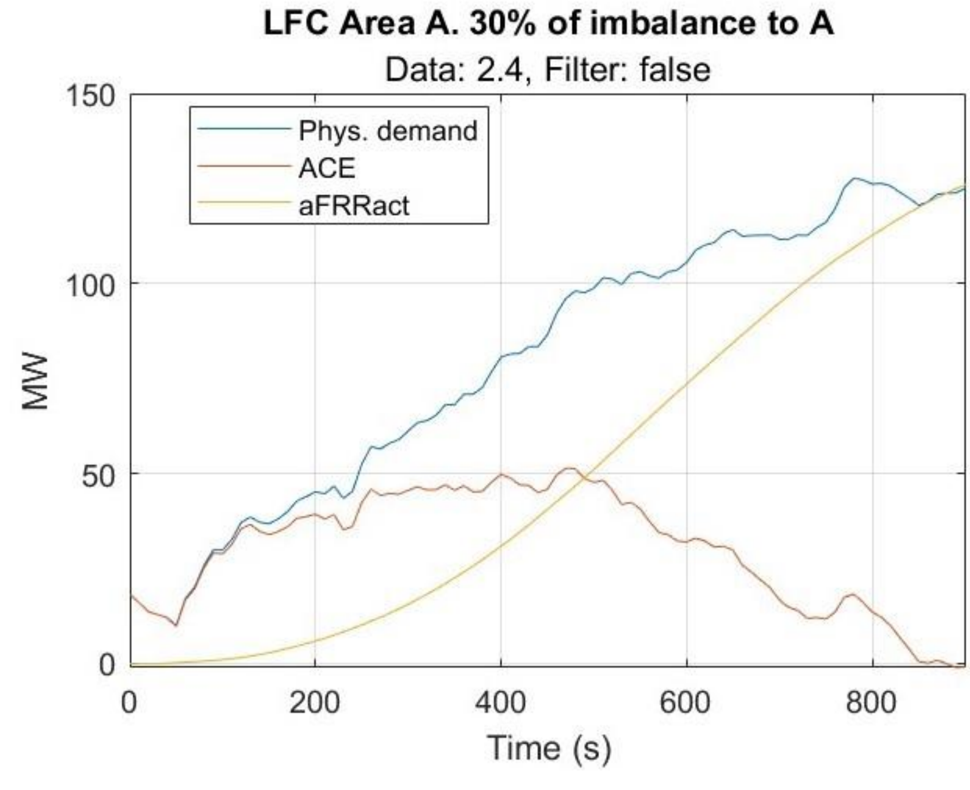


Figure 64. Alternative 3, data 2.4, no filtering, LFC area A.

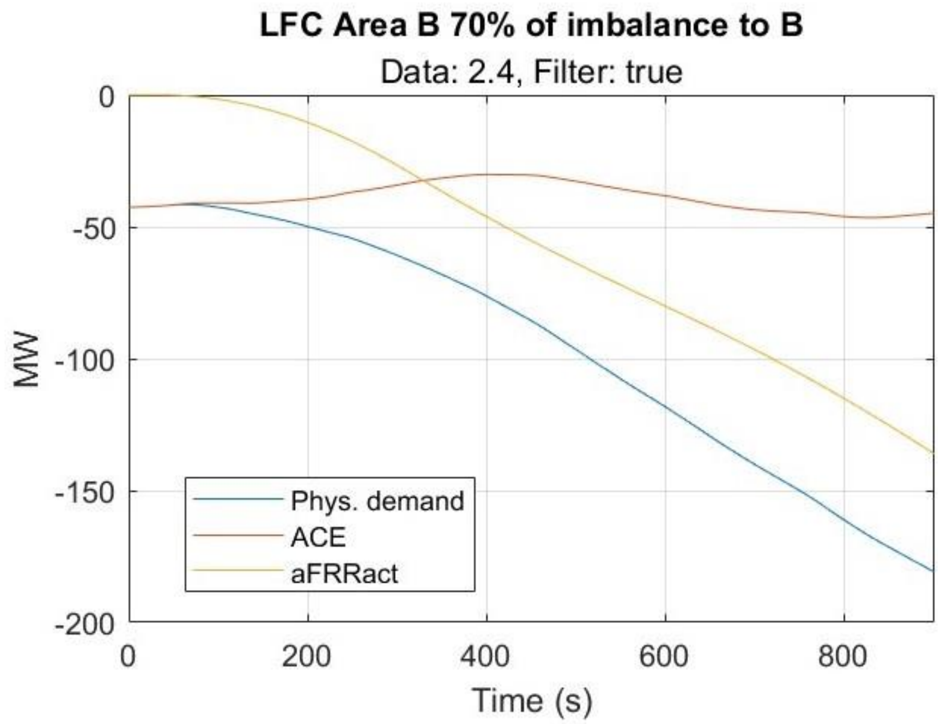


Figure 65. Alternative 3, data 2.4, filtering, LFC area B.

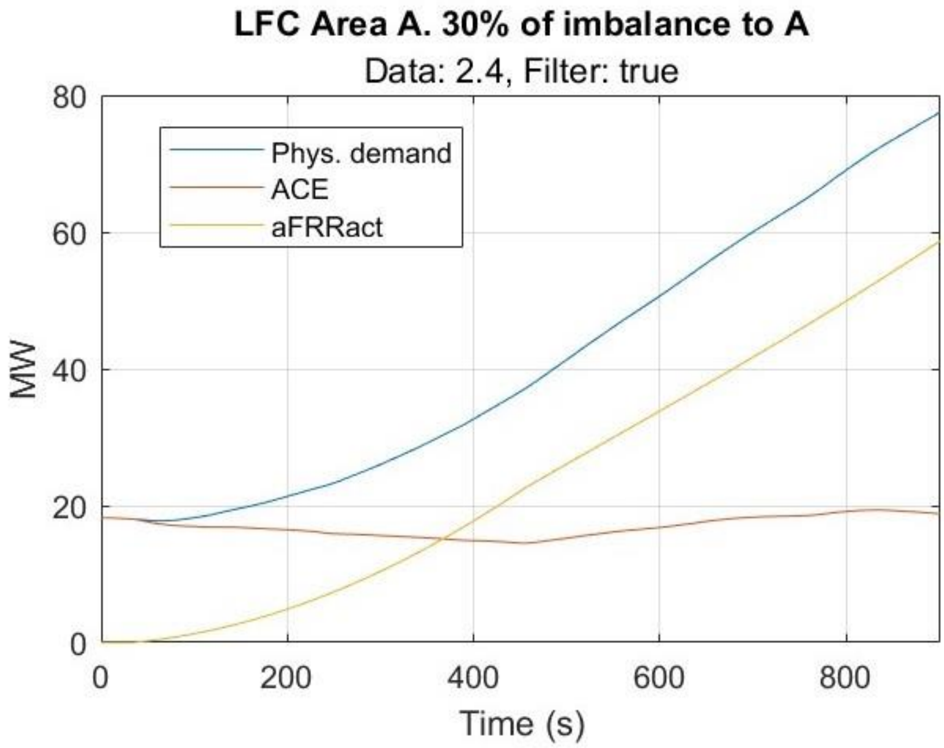


Figure 66. Alternative 3, data 2.4, filtering, LFC area B.

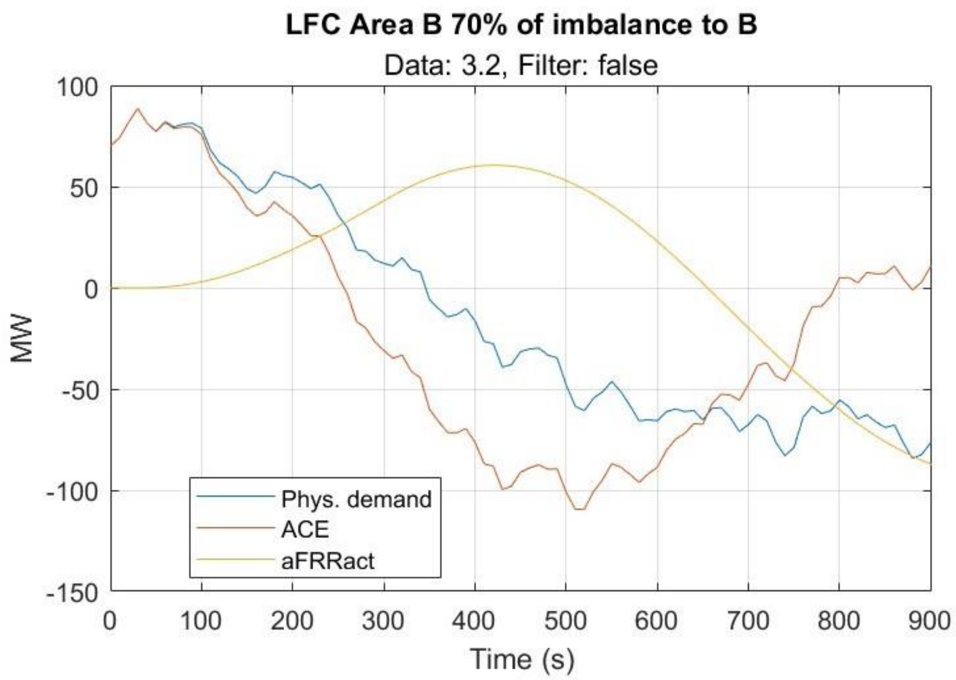


Figure 67. Alternative 3, data 3.2, no filtering, LFC area B.

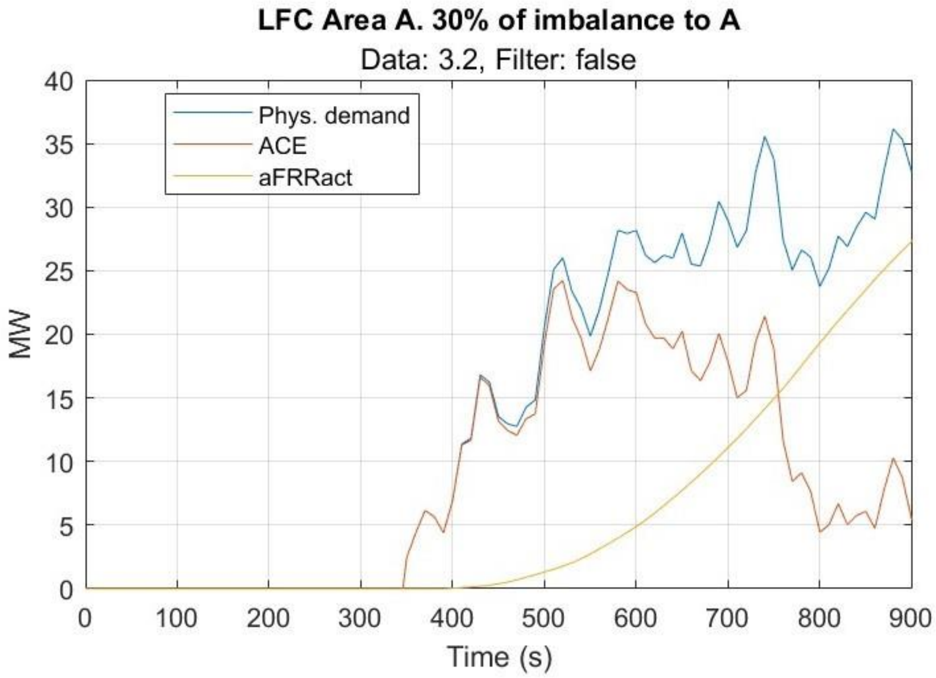


Figure 68. Alternative 3, data 3.2, no filtering, LFC area A.

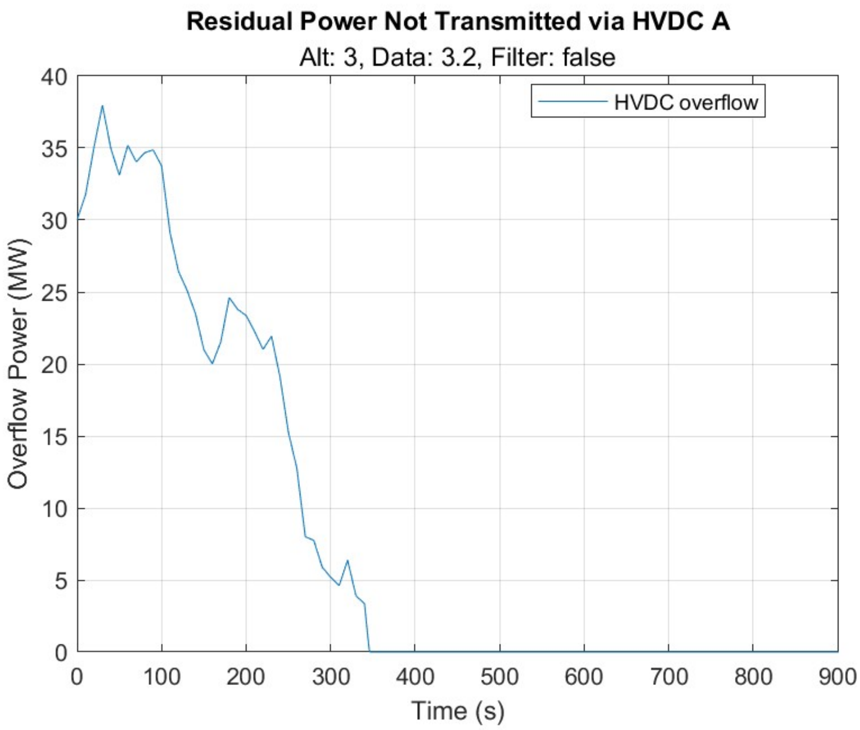


Figure 69. Alternative 3, data 3.2, no filtering, residual power not transmitted to LFC area A.

**Dataset 3.2 filtered**

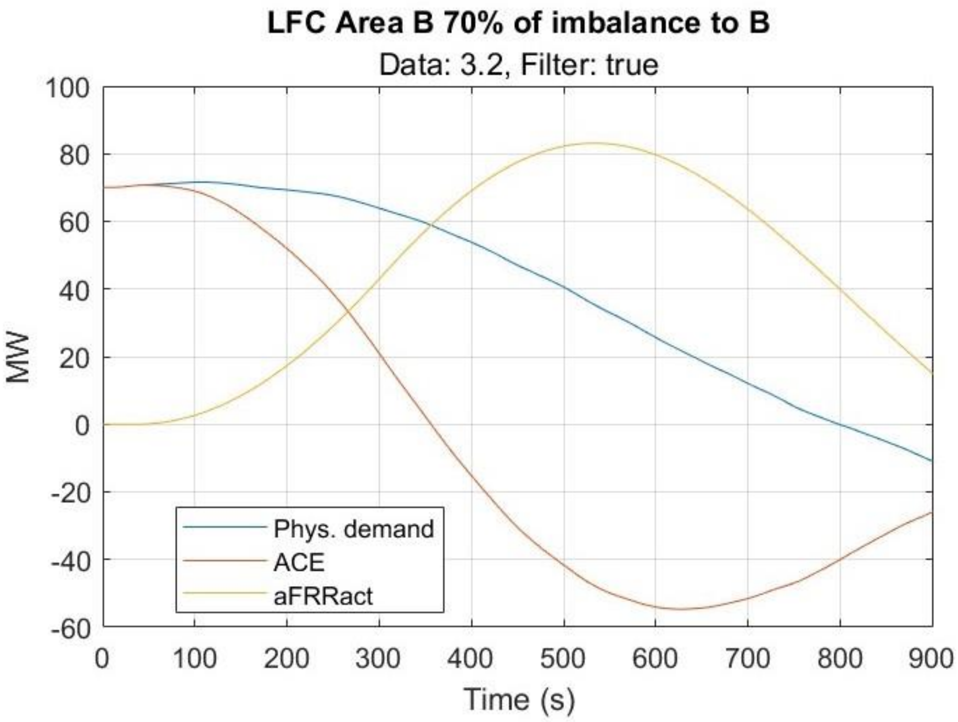


Figure 70. Alternative 3, data 3.2, filtering, LFC area B.

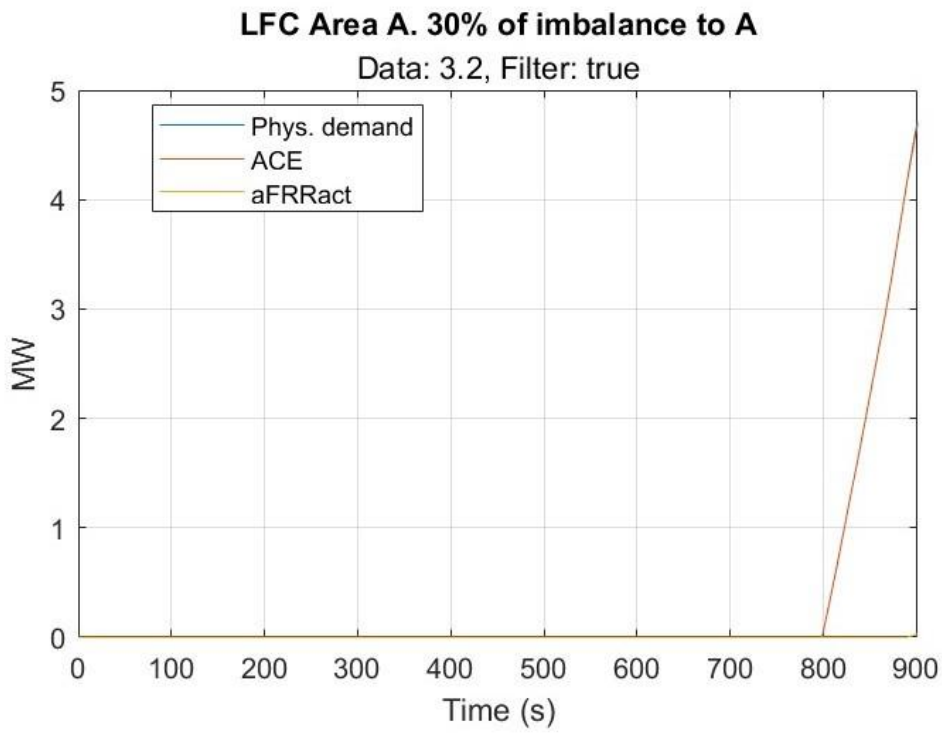


Figure 71. Alternative 3, data 3.2, filtering, LFC area A.

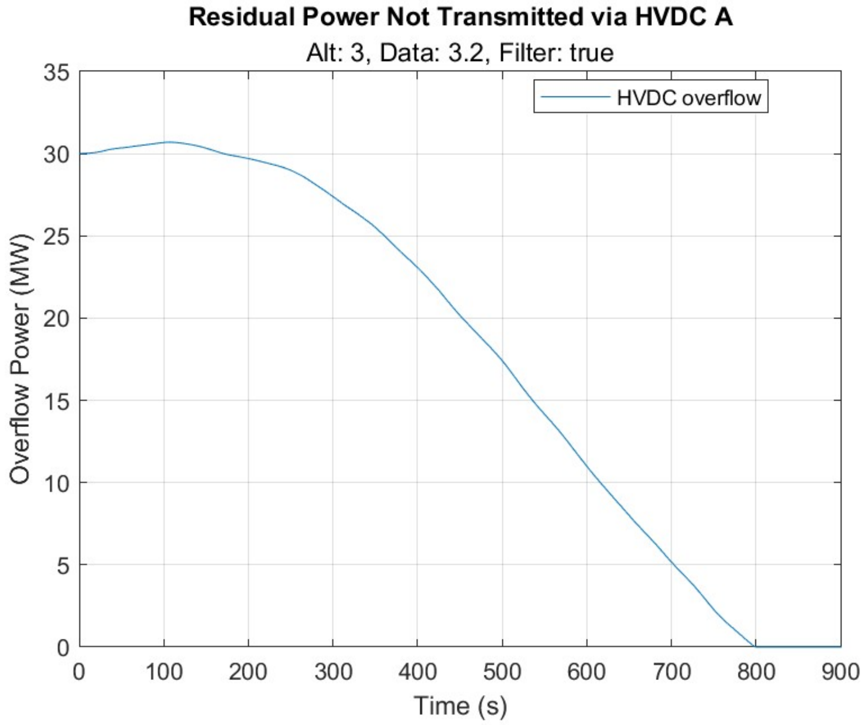


Figure 72. Alternative 3, data 3.2, filtering, residual power not transmitted to LFC area A.

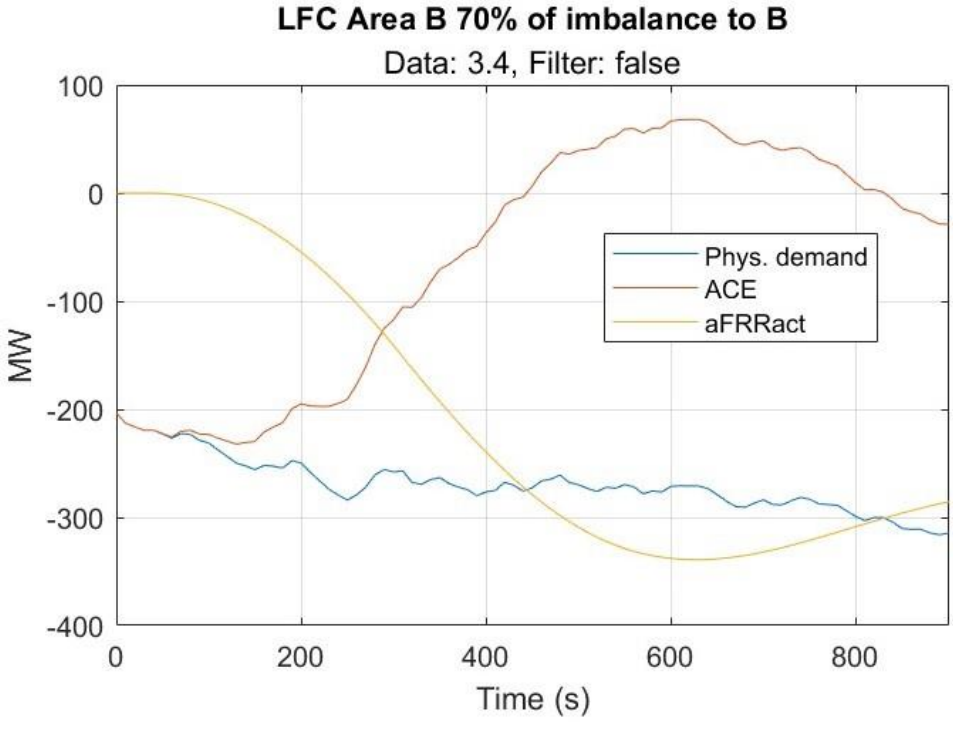


Figure 73. Alternative 3, data 3.4, no filtering, LFC area B.

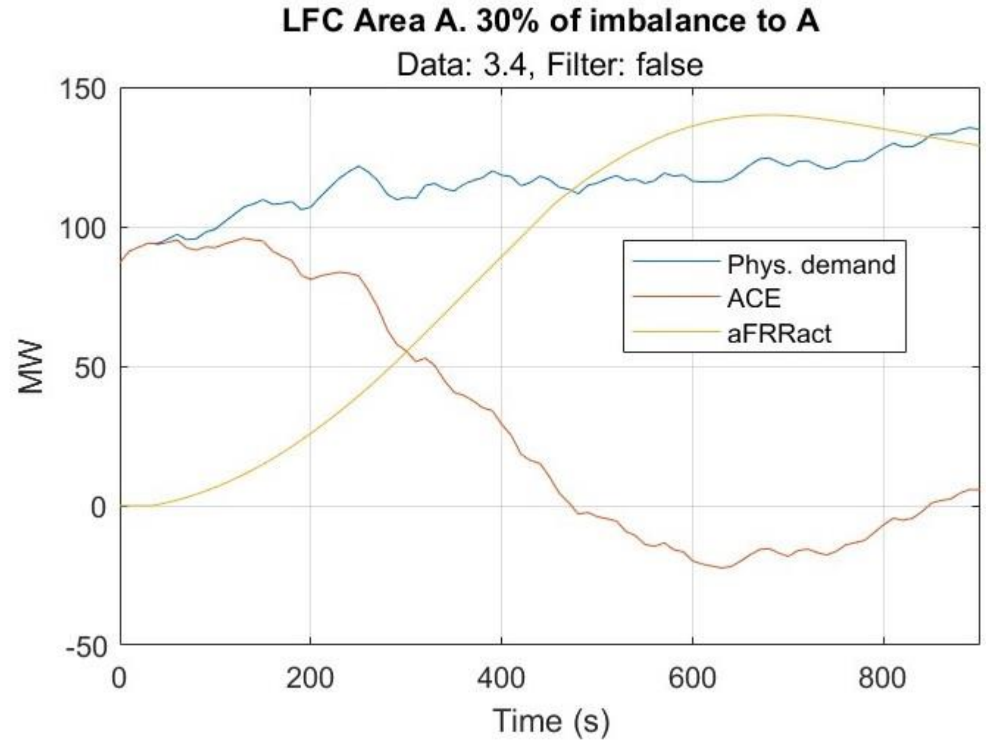


Figure 74. Alternative 3, data 3.4, no filtering, LFC area A.

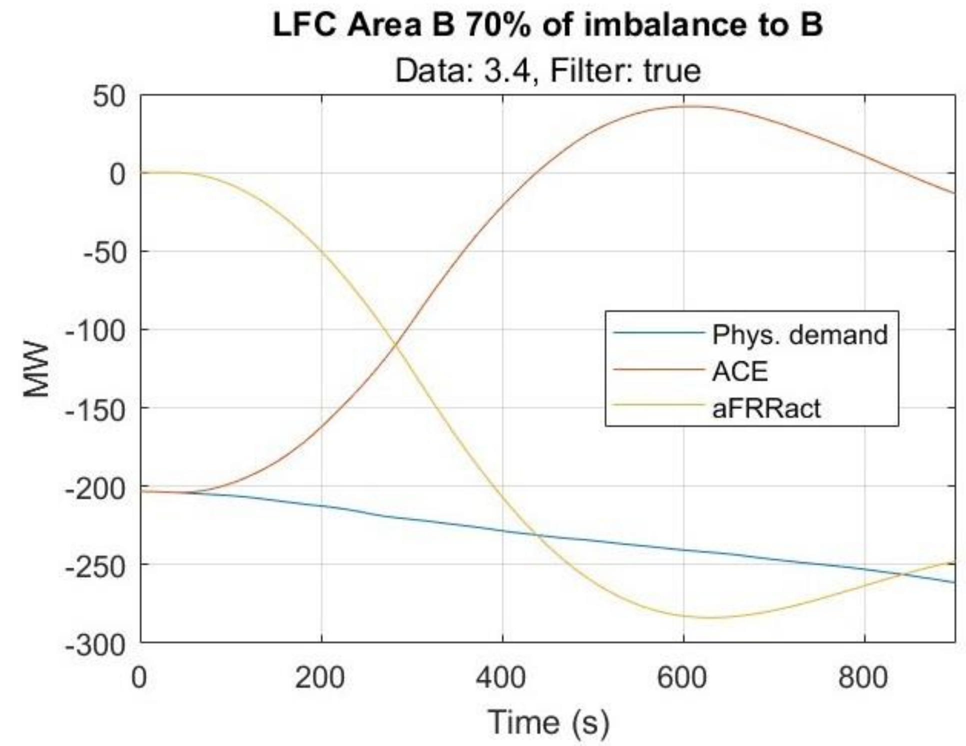


Figure 75. Alternative 3, data 3.4, filtering, LFC area B.

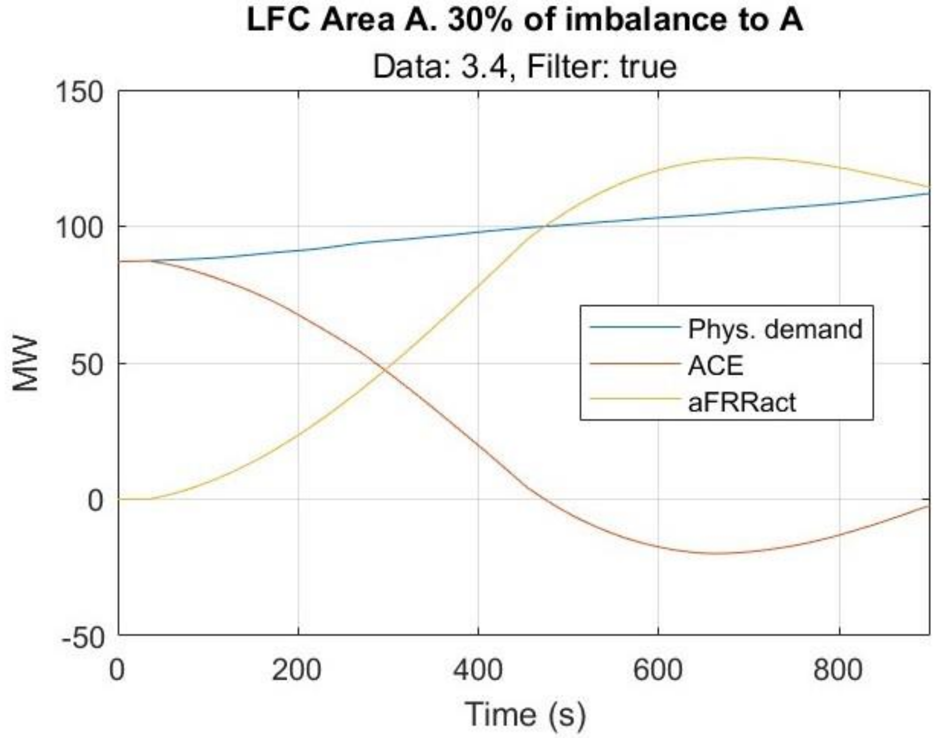


Figure 76. Alternative 3, data 3.4, no filtering, LFC area A.

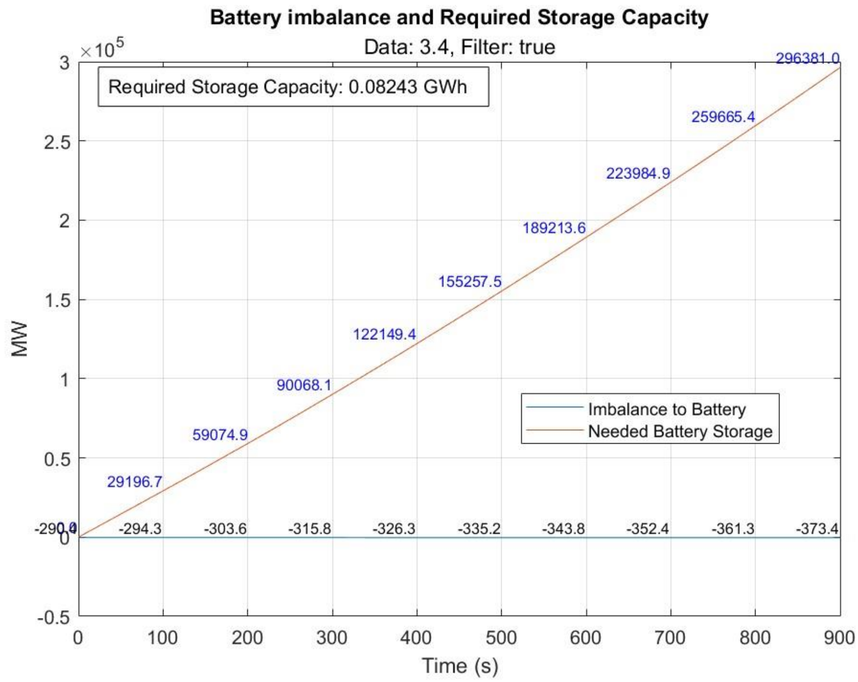


Figure 77. Alternative 4, data 3.4, filtering